Estimating Errors in Analog Quantum Simulations

Zur Erlangung des akademischen Grades einer
DOKTORIN DER NATURWISSENSCHAFTEN
von der KIT-Fakultät für Physik des
Karlsruher Instituts für Technologie (KIT)

genehmigte
DISSERTATION
von

M. Sc. Iris Schwenk (geb. Conradi)

aus Wiesbaden

Dissertation

Estimating Errors in Analog Quantum Simulations

M. Sc. Iris Schwenk (geb. Conradi)

23. November 2018

KIT-Fakultät für Physik
am Karlsruher Institut für Technologie (KIT)

Acknowledgments

List of publications

I. Schwenk, I., Reiner, J.-M., Zanker, S., Tian, L., Leppäkangas, J. & Marthaler, M. *Reconstructing the ideal results of a perturbed analog quantum simulator*. Phys. Rev. A **97,** 042310 (2018) (cit. on pp. 61, 64, 85).

II. Zanker, S., Schwenk, I., Reiner, J.-M., Leppäkangas, J. & Marthaler, M. *Analyzing the spectral density of a perturbed analog quantum simulator using the Keldysh formalism*. Phys. Rev. B **97,** 214301 (2018) (cit. on pp. 65, 85).

III. Reiner, J.-M., Zanker, S., Schwenk, I., Leppäkangas, J., Wilhelm-Mauch, F. K., Schön, G. & Marthaler, M. *Effects of gate errors in digital quantum simulations of fermionic systems*. Quantum Sci. Technol. **3,** 045008 (2018) (cit. on pp. 11, 18).

IV. Leppäkangas, J., Braumüller, J., Hauck, M., Reiner, J.-M., Schwenk, I., Zanker, S., Fritz, L., Ustinov, A. V., Weides, M. & Marthaler, M. *Quantum simulation of the spin-boson model with a microwave circuit*. Phys. Rev. A **97,** 052321 (2018) (cit. on p. 10).

V. Schwenk, I., Zanker, S., Reiner, J.-M., Leppäkangas, J. & Marthaler, M. *Estimating the Error of an Analog Quantum Simulator by Additional Measurements*. Phys. Rev. Lett. **119,** 240502 (2017) (cit. on pp. 45, 85).

VI. Schwenk, I. & Marthaler, M. *Distortion of a reduced equilibrium density matrix: Influence on quantum emulation*. Phys. Rev. B **93,** 014305 (2016) (cit. on pp. 18, 28, 33, 35, 38, 42, 44, 84).

VII. Tian, L., Schwenk, I. & Marthaler, M. *Detector Readout of Analog Quantum Simulators*. arXiv: `1612.07419v1` (2016) (cit. on pp. 62, 85).

Best Poster Prize for „Recovering the ideal results of a perturbed analog quantum simulator", 635th WE-Heraeus Seminar - Scalable Architectures for Quantum Simulation.

Contribution (40%) to a software (MolQC) consisting of code to simulate molecules and to implement simulations on quantum computers that is licenced by KIT.

Contents

1. Introduction

With the immense progress in quantum hardware development in the last years [1] the long-term dream of quantum computing appears to become reality [2]. Quantum chips of significant size have been presented or are even available via cloud access [3, 4]. The fact, that it is computationally very expensive to study large quantum systems numerically is a driving force for the efforts in the field of quantum information. The Hilbert space of a quantum problem grows exponentially with the system size. Therefore, the exact simulation of even moderate size quantum systems is impossible on present-day computers. For example, the storage of the state of 40 two-level systems requires approximately four terabytes of memory, and for 70 two-level systems we need to store an amount of information that equals the amount of information stored by humankind in 2007 [5]. The usage of quantum systems, that themselves provide this exponentially increasing state space as a memory, may solve the problem. A fundamental prerequisite for quantum information processing is that the quantum state remains intact over the computation time, which means that the decoherence times of the qubits, the central building blocks of quantum computers, are longer than the processing time needed for the gates [6]. A substantial breakthrough in quantum hardware development was achieved when the quality of the qubits reached the so-called quantum error correction threshold [7], which means that it is fundamentally possible to build fault-tolerant logical qubits out of the noisy physical qubits. On the other hand, at the moment thousands of qubits are needed to form one logical qubit. With this, a fully error-corrected quantum computer is still far out of reach.

At this stage, an important question is, how to make use of the immense progress in quantum hardware development at present before a fully error-corrected universal quantum computer is available [8]. An important field of application is the simulation of

quantum systems or models [5]. In general, two different approaches are discussed. Digital quantum simulation, which is a gate-based approach which would also be used on a fault-tolerant universal quantum computer. A possible application is the simulation of the time evolution of a quantum system in discretized time steps [9]. Another promising approach is analog quantum simulation, where the system of interest is emulated by an artificial quantum system. A simple example is the simulation of coupled two-level systems using qubits [10]. Both gate-based systems and analog quantum simulators can be build based on many different physical systems [11]. A multitude of experiments have been done to improve the abilities of controlling this artificial quantum systems to pave the way to realize simulations of systems that are computationally intractable. With superconducting qubits it is for example possible to study the spin-boson model in numerically inaccessible regimes [IV] in an analog quantum simulation. Very spectacular experiments have been performed based on cold gases. For example, frustrated spin systems [12] have been emulated and the limit of classical computation has been reached [13]. But analog quantum simulation is not restricted to solid state systems, it is for example even possible to study problems from cosmology [14]. Furthermore, it is possible to combine the advantages of analog simulations and gate based calculations in so-called digital-analog simulations [15].

Using a quantum simulator we aim to solve problems that are not solvable numerically on classical computers. For interesting problems, usually it is not even possible to verify the accuracy of the results using a classical computer. For near-term digital quantum simulators quantum error correction is not accessible, and for analog quantum simulation, it is fundamentally not applicable. Therefore, reliability is the crucial requirement for useful quantum simulations [16, 17]. Several techniques exist to get a feeling of the reliability. For example, the cross validation method relies on building simulators for the same problem on different physical realizations [18]. Assuming that errors in different physical realizations are not the same, concordant results on the different simulators indicate reliability. For interesting quantum simulations a comparison to numerical results is, by construction, not possible. However, a comparison may be possible if the

quantum simulator is tuned to an appropriate parameter regime [19, 20]. Furthermore, the accuracy of a time evolution can be checked by running the time evolution forward and backward, verifying that the initial state is reached again [17]. This method requires double the coherence time, and it depends on the state. All these methods only give a feeling of reliability of the quantum simulation. To lay the foundation of reliable quantum simulations it is important to quantitatively understand the influence of errors [III, 21–23]. Furthermore, developing a measure for the reliability, or methods to mitigate errors [24–26] can substantially improve the use of quantum simulation. Some mitigation techniques exploit symmetries, others are based on perturbative arguments, and most of them have been developed for digital quantum simulation. The ultimate goal would be to find an alternative to quantum error correction that requires less overhead on the quantum system. That would allow for reliable quantum simulations of interesting systems in the near future, where only small qubit systems will be available. In general, this is certainly a difficult task. Therefore, even proposals to the reliability that have significant limitations can be important.

The focus of this thesis is estimating, and potentially improving, the reliability of analog quantum simulations. Starting from understanding the influence of errors, we next present a method to check for the reliability of a simulator, and in the end, we show that it is possible, under specific circumstances, to reconstruct the unperturbed result. All three parts are based on the same assumption. We regard external degrees of freedom as the sources of errors in quantum simulations. Quantum simulators are artificial quantum systems. They are not perfectly isolated from the environment, at least for the purpose of control and readout. We consider the quantum simulator connected to these unwanted environmental degrees of freedom. This system-bath approach, alongside with some theoretical foundations, is described in chapter 2. Another similarity between all parts presented in this thesis is that they are based on perturbation expansions. In chapter 3 we study the influence of external degrees of freedom on the state of the simulator in thermal equilibrium. For this purpose, we derive an expression for the reduced density matrix. With this, we can study the reduced density matrix depending on the strength

of the coupling to the perturbation. Comparing the result to the density matrix of the ideal simulator allows us to understand the influence of environmental degrees of freedom on the state of the simulator. For example, we can examine the change of the eigenbasis induced by the external degrees of freedom, or study quantum properties like entanglement depending on the coupling strength. These calculations require that the eigenstates and eigenenergies of the simulated system are known. Therefore, this method is applicable to systems that can be solved with classical computers. Consequently, this method helps to understand errors in analog quantum simulations but has no ability to verify the reliability of a simulation of an interesting system.

In chapter 4 we study a time-dependent quantum simulator. Apart from analog quantum simulations in non-equilibrium, this covers in principal also digital quantum simulations. In contrast to the previous chapter, we do not study the density matrix from which a calculation of matrix elements is possible. Instead, we directly examine the expectation value of an operator and the variation due to the coupling to environmental degrees of freedom. Using a lowest order perturbation expansion we derive an equation that allows us to estimate the size of the error induced by external degrees of freedom via additional measurements on the quantum simulator.

In chapter 5 we again focus on calculating directly measurable quantities. Here, we are interested in correlators instead of expectation values. In particular, we focus on a very specific correlator, namely, the correlator of the operator that mediates the coupling to external degrees of freedom. This allows us, under very specific circumstances, to derive an equation that connects the perturbed correlator with the ideal correlator. In particular, we assume that higher-order correlators can be written in terms of two-time correlators. With this, it is possible to reconstruct the ideal value of the correlator based on measurements of the perturbed correlator and the bath. Furthermore, we explain how to verify the central assumption for the correlators for this derivation in an experiment.

In principle, all the parts presented in this thesis are very general. Due to the fact that they have to apply to a general quantum simulator, we make no assumptions for the

Hamiltonian of the simulator. With this, the presented work should be of interest in a larger field of open quantum systems. In the context of quantum simulations, we present techniques that help to understand the influence of errors and to verify or enhance the reliability of a simulation.

2. Theoretical background and general approach to study errors in analog quantum simulations

The purpose of this chapter is to introduce our approach to analyze errors in quantum simulations which forms the basis for all chapters presented in this thesis. A quantum simulator is an artificial quantum system with the possibility to control its properties and to read-out results. At least due to the control and readout, it is unavoidable that the system is coupled to external degrees of freedom, which we call bath. To understand errors in a quantum simulation it is necessary to consider these external degrees of freedom and the coupling to the simulator. Using a system-bath approach we separate the Hamiltonian into three parts: simulator, bath, and coupling. Expansions in the coupling Hamiltonian allow us to incorporate the effect of the external degrees of freedom perturbatively. With this, we can understand the influence of noise on the results of the simulation.

2.1. System-bath approach

Building an analog quantum simulator means creating an artificial quantum system that represents the Hamiltonian of the system that should be simulated. These artificial quantum systems can be build based on many physical realizations like, e.g., superconducting circuits, trapped ions, semiconductor quantum dots, or NV-centers in diamond.

Independent of the physical realization it is unavoidable that external degrees of freedom are coupled to the system that was intended to build. At least for the purpose of readout and controllability, it is necessary to introduce couplings to the environment. In addition, there are also undesired couplings to external degrees of freedom that affect the system. Superconducting circuits are disturbed, e.g., by impurities in the substrate, electronic excitations or coupling to external wiring [27]. A main source for decoherence in trapped ion systems are fluctuating magnetic fields [28]. The same sources of noise also occure in digital quantum simulators. In general, it is possible to describe the influence of external degrees of freedom using a system-bath approach. Quantum systems are never isolated. Therefore, the influence of an environment on the state of a quantum mechanical system is studied intensively in the field of open quantum systems, for example using master equations [29]. In the context of adiabatic quantum computation or gate based quantum computation the influence of external degrees of freedom has been studied [25, 30]. To study the effect of external degrees of freedom on a quantum simulator we consider them as an environment. The full system is given by the Hamiltonian,

$$H = H_S + \lambda_B H_C + H_B \,. \tag{2.1}$$

with $\lambda_B = 1$. H_S describes the perfect artificial quantum system that builds the quantum simulator. All external degrees of freedom are collected in the bath Hamiltonian H_B. The coupling of the external degrees of freedom to the system is given by H_C. This setting is illustrated in Fig. 2.1. With $\lambda_B = 0$ we describe the unperturbed system. In principle, this model is capable to describe quantum simulators coupled to arbitrary perturbations. The following very simple form of the coupling Hamiltonian,

$$H_C = \hat{O}\hat{X} \tag{2.2}$$

is used to explain the fundamental ideas in the following chapters. Here, $\hat{O}$ describes the operator of the system that mediates the coupling to the bath. And $\hat{X}$ is an operator
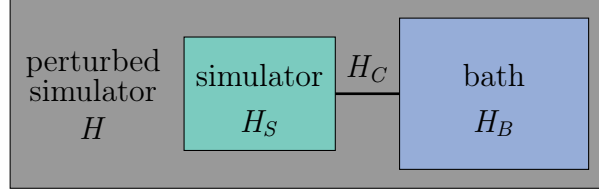
Figure 2.1.: This figure gives a schematic overview of the general setting considered in this work. The full system described by Hamiltonian H is formed by the simulator (H_S) that is coupled to external degrees of freedom, which we call bath (H_B). The coupling is characterized by the coupling Hamiltonian H_C.

of the bath. In practice, a system of qubits or resonators is not coupled to a bath via a single operator. In fact, each element is coupled to an individual bath $H_B = \sum_{i=1}^{N} H_B^i$ with $[H_B^i, H_B^j] = 0$ via,

$$H_C = \sum_{i=1}^{N} \hat{O}^i \hat{X}^i \,. \tag{2.3}$$

A generalization to such a coupling Hamiltonian is described in all of the following works. In the predominant part of the following chapters, we assume the bath to be bosonic, so that $\hat{X}$ is a linear combination of bosonic creation and annihilation operators. For example, phonons or the electromagnetic field can be described in this way. A bath of bosonic modes allows us to describe every perturbation where the fluctuations follow a Gaussian distribution. In most systems, non-Gaussian corrections remain small [31, 32]. Fluctuating background charges [33] or quasiparticle tunneling [34, 35] are examples for a source of fermionic perturbations in superconducting qubits. The transfer to a fermionic bath is possible for all works presented in the following chapters with only a few adjustments. In chapter 5 we also introduce restrictions to the system operator $\hat{O}$. Here, we assume $\hat{O}(t)$ to behave bosonic under time-ordering.

In chapter 4 we allow the Hamiltonian of the simulator to be time dependent. Therefore, these results are in principle also applicable to digital quantum simulations. The works in chapter 3 and 5 are focused on analog quantum simulations in thermal equilibrium.
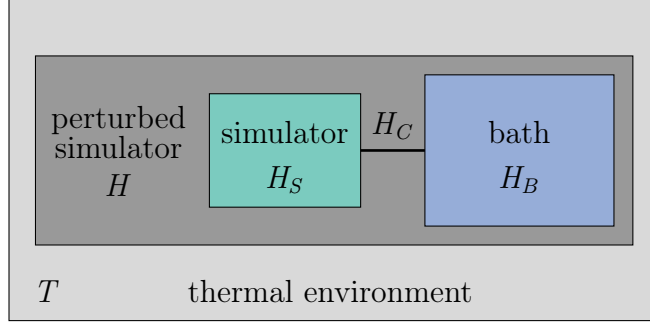
Figure 2.2.: This figure illustrates the general setting of a perturbed simulator in thermal equilibrium. The simulator is connected to a bath that represents the external degrees of freedom creating the perturbation. Additionally, this perturbed simulator couples infinitesimally small to another bath that has no other effect on the system than to create a thermal equilibrium with temperature T.

In this case, the full system consisting of system and bath is coupled infinitesimally weak to another bath that creates the thermal equilibrium. Since it is coupled infinitesimally weak, the bath has no other effect than creating the equilibrium [VI, 30, 36]. This situation is depicted in Fig. 2.2.

Apart from perturbations due to external degrees of freedom other sources of noise can be present in quantum simulations. In case of a digital quantum simulation, imperfect execution of gates results in errors. The effect of gate errors was studied by Reiner et al. in [III]. The work presented in chapter 4 can be applied to gate errors. Furthermore, imperfect fabrications can lead to errors in the system that are described by disorder. This is not the focus of this thesis, but it is covered by the work presented in chapter 4.

2.2. Influence of the bath in different coupling limits

In comparison to the ideal results, the outcome of the simulation will change due to the influence of the external degrees of freedom. A perfect simulator would yield results based on the state of the system described by H_S. The values without perturbations

are denoted by $\langle \ldots \rangle_0$, since $\lambda_B = 0$. In reality, the measurement is performed on the full system. Therefore, the results are taken with respect to the state of the full system. The result of a simulation could, for example, be an expectation value or a correlator. In general, they will differ from the ideal values,

$$\langle \hat{A}(t) \rangle \neq \langle \hat{A}(t) \rangle_0 \qquad \langle \hat{A}(t)\hat{B}(0) \rangle \neq \langle \hat{A}(t)\hat{B}(0) \rangle_0 \ , \tag{2.4}$$

where A and B are observables of the system.

In the case of thermal equilibrium, the state of the ideal system is given by the equilibrium density matrix

$$\rho_S = e^{-\beta H_S} \frac{1}{\mathrm{Tr}(e^{-\beta H_S})} \ , \tag{2.5}$$

with the inverse temperature $\beta = {}^1\!/\!{}_{k_B T}$. The full density matrix ρ describes the state of the system consisting of the simulator coupled to the external degrees of freedom,

$$\rho = e^{-\beta H} \frac{1}{\mathrm{Tr}\left(e^{-\beta H}\right)} \ . \tag{2.6}$$

A trace over the external degrees of freedom yields the reduced density matrix of the system $\mathrm{Tr}_B(\rho) = \tilde{\rho}_S$, which describes the state of simulator in presence of noise. In general, this density matrix will differ from the unperturbed one, so that the expectation values differ,

$$\langle A \rangle = \mathrm{Tr}\left(\rho A\right) = \mathrm{Tr}_S\left(\tilde{\rho}_S A\right) \neq \langle A \rangle_0 \ . \tag{2.7}$$

If the coupling of the external degrees of freedom to the system is infinitesimally small, the reduced density matrix $\tilde{\rho}_S$ will be diagonal in the eigenbasis of the system, meaning $[\tilde{\rho}_S, H_S] = 0$. So for small coupling strength, we expect that the external degrees of freedom only alter the occupation numbers of the eigenstates of the system, which can be described by renormalized energies. In case of an infinitesimally strong coupling, the

reduced density matrix will be diagonal in the eigenbasis of the coupling Hamiltonian [37, 38], $[\tilde{\rho}_S, H_C] = 0$. For intermediate coupling strength, we, therefore, suppose a change in the eigenbasis of the reduced density matrix compared to the ideal system, if the diagonal basis of H_S and H_C differ.

In the context of this work, we are interested in the case where the coupling to the external degrees of freedom results in a significant adjustment of the simulation results, which affects the reliability of the simulation. A small change of the occupation could perhaps preserve the reliability of the measurement results. Whereas a fundamental change of the eigenbasis may jeopardize the reliability. In chapter 3, we study the influence of the external degrees of freedom on the state of the perturbed simulator described by the reduced density matrix. Herewith, we show, that the influence of the external degrees of freedom on the simulator can be significant. In chapter 4, we examine the reliability of the measurement of a time-dependent expectation value on a quantum simulator in the limit of small noise. The influence of perturbations on a correlator is the issue of chapter 5. This work is valid for intermediate coupling strength and furthermore allows for a reconstruction of the ideal result under specific circumstances.

2.3. Study the influence of the bath using perturbation theory

The foundation of the analyses of the effect of perturbations on a quantum simulator presented in the following chapters are perturbation expansions in the coupling Hamiltonian H_C. To perform the expansion in the context of the different quantities under consideration we use various techniques in real time or in imaginary time. However, in any case, we introduce the interaction picture. For example in a consideration in

real-time the time evolution is given by

$$U_{\lambda_B}(t, t_0) = \mathcal{T} \exp\left(-i \int_{t_0}^{t} dt' \, H(t')\right), \tag{2.8}$$

where $\mathcal{T}$ denotes the time-ordering operator $(t > t_0)$. Time evolution operators in imaginary time are denoted by S_{λ_B}. U_1 describes the time evolution of the full system. The time evolution of the ideal system is expressed by U_0. In expectation values and correlators of the full system $\langle \ldots \rangle$, the evolution operator with $\lambda_B = 1$ is used. In $\langle \ldots \rangle_0$ the ideal time evolution with $\lambda_B = 0$ applies. A transformation to the interaction picture is achieved with $\hat{B}_I(t) = U_0(t_0, t) \hat{B} \, U_0(t, t_0)$. The index I is dropped inside $\langle \ldots \rangle_0$, since the appropriate time evolution operator is given implicitly. Looking at the full system in the interaction picture, the time evolution operator is

$$\mathcal{U}(t, t_0) = \mathcal{T} \exp\left(-i \int_{t_0}^{t} dt' \, H_{C,I}(t')\right). \tag{2.9}$$

In imaginary time the equivalent operator is denoted by $\mathcal{S}$. The perturbative methods used in the following chapters perform an expansion of such time evolution operators of H_C in terms of the coupling Hamiltonian H_C.

In the resulting equations, the properties of the bath are described by the bath correlators $\langle \hat{X}_i(t) \hat{X}_i(0) \rangle_0$ or its spectral densities. The works presented in the following chapters rely on an appropriate knowledge of these quantities. We have to emphasize that we need to characterize the correlator of the bath independent of the simulator [39], as indicated with index 0. For example, in the case of a simulator build from tunable qubits well established spectroscopical methods can be used to probe the properties of the baths. For this purpose, the qubits are decoupled so that the properties of the individual baths are accessible. In the case of a large number of coupled superconducting flux qubits, used to simulate spin systems [40, 41], it is possible to characterize the noise independent of the system. The simulator is described by $H_S = \frac{1}{2} \sum_i h_i \sigma_x^i + \sum_{ij} J_{ij} \sigma_z^i \sigma_z^j$, where h_i and J_{ij} are chosen to realize a certain model and σ_k^i are the Pauli matrices of

qubit i. Assuming Markovian noise for qubits the characterization of the noise spectral density of individual qubits is described in Ref. [42] and the bath correlators are known relatively well [43]. Furthermore, it is known that in this systems the noise is coupled via $\hat{O}^i = \sigma_z^i$.

2.4. Diagrammatic expansion for Green's functions of bosonic operators

The basis for the diagrammatic expansions in the following chapters is the expansion of the time evolution operator in interaction picture. In this section, we show where this time evolution operator appears in standard diagrammatics. Standard diagrammatics regards Green's functions of fermionic or bosonic field operators. Three types of diagrammatic techniques are common: zero temperature diagrammatic, Matsubara diagrammatic for equilibrium situations, and Keldysh diagrammatic for non-equilibrium situations. Here, we shortly show the derivation of the main equation in zero temperature diagrammatics. However, we focus on Green's functions of general bosonic operators, not on Green's functions of field operators. With this, we derive the basis for chapter 5. Detailed explanations of standard diagrammatic techniques can be found in the literature, for example in [44, 45].

We regard the system-bath setting as described in Eq. (2.1). For the purpose of this derivation, we focus on the simple coupling Hamiltonian Eq. (2.2). A generalization to Eq. (2.3) is directly possible. We are interested in the correlator $\langle \mathcal{T} \hat{O}(t) \hat{O}(0) \rangle$ of the full system ($\lambda_B = 1$) at zero temperature. Therefore, $\langle \ldots \rangle$ describes the expectation value of the ground state of the full system. This correlator is proportional to the perturbed Green's function of the coupling operator $\hat{O}$. The goal is to express this correlator in terms of quantities of the ideal system ($\lambda_B = 0$, $\langle \ldots \rangle_0$). $\mathcal{T}$ is the time-ordering operator. In the context of diagrammatic techniques, two different kinds of time-ordering operators are of importance. On one hand, the Dyson time-ordering operator occurs in

the Dyson series that forms the basis for time evolution operators with time-ordered exponentials like Eq. (2.9). Under this time-ordering operator, arbitrary reordering of operators is allowed. On the other hand, in the definition of Green's functions the Wick time-ordering operator occurs. In this case, a permutation of fermionic field operators results in a prefactor -1. Interchanging bosonic field operators or products of even numbers of fermionic field operators produces no additional prefactors. In standard diagrammatics, the difference of this time-ordering operators is of no consequence due to the regarded Green's functions and Hamiltonians, especially because the Hamiltonian describing the perturbation is a product of four field operators. To be able to transfer the derivation of standard diagrammatics to the more general case of Green's functions of coupling operator $\hat{O}$ we assume that operator $\hat{O}_I(t)$ behaves bosonic under time-ordering, which means that permutations of operators yield no sign changes. With this, the two kinds of time-ordering operators are interchangeable, as it is the case in standard diagrammatics.

The correlator $\langle \mathcal{T} \hat{O}(t) \hat{O}(0) \rangle$ involves the time evolution under the full Hamiltonian. We introduce the interaction picture (see Eq. (2.9))

$$\langle \mathcal{T} \hat{O}(t) \hat{O}(0) \rangle = \langle \mathcal{T} \mathcal{U}(0,t) \hat{O}_I(t) \mathcal{U}(t,0) \hat{O}_I(0) \rangle . \tag{2.10}$$

Assuming the coupling (H_C) to be turned off adiabatically for times $\pm\infty$ it is possible to write the correlator based on the expectation value of the ground state of the unperturbed system ($\lambda_B = 0$)

$$\langle \mathcal{T} \hat{O}(t) \hat{O}(0) \rangle = \langle \mathcal{U}(-\infty, 0) \mathcal{T} \mathcal{U}(0,t) \hat{O}(t) \mathcal{U}(t,0) \hat{O}(0) \mathcal{U}(0,-\infty) \rangle_0 . \tag{2.11}$$

Under $\langle \ldots \rangle_0$ it is implied that the time-evolution is according to the free system. Therefore, index I is dropped. A rearrangement of operators under the time-ordering operator

leads to

$$\langle \mathcal{T} \hat{O}(t)\hat{O}(0) \rangle = \frac{\langle \mathcal{T}\mathcal{U}(\infty)\hat{O}(t)\hat{O}(0) \rangle_0}{\langle \mathcal{U}(\infty) \rangle_0} \, , \qquad (2.12)$$

where we introduce $\mathcal{U}(\infty) = \mathcal{U}(\infty, -\infty)$. The expansion of $\mathcal{U}(\infty)$ in terms of H_C in this equation is the starting point for diagrammatics. It leads to correlators with different numbers of operators $\hat{O}$ and $\hat{X}$. A crucial assumption for diagrammatics is that Wick's theorem is true for the operators involved. Wick's theorem allows us to write higher-order correlators as sums of products of two-time correlators. This involves that expectation values of odd numbers of operators are assumed to be zero. Wick's theorem is true for fermionic and bosonic field operators as they appear in standard diagrammatics. If we assume the bath to be bosonic it is also clear that it is true for operator $\hat{X}$. The validity of Wick's theorem for $\hat{O}$ is a non-trivial assumption and is discussed in detail in chapter 5. Since we require a bosonic behavior of $\hat{O}$ under time-ordering we assume a bosonic Wick's theorem to hold, which means that all terms have a positive sign. For operator $\hat{O}$ this means that we repeatedly apply

$$\begin{aligned}
\langle \mathcal{T}\hat{O}(t_1)\hat{O}(t_2)&\ldots\hat{O}(t_{n-1})\hat{O}(t_n) \rangle_0 \\
&= \langle \mathcal{T}\hat{O}(t_1)\hat{O}(t_2) \rangle_0 \langle \mathcal{T}\hat{O}(t_3)\ldots\hat{O}(t_{n-1})\hat{O}(t_n) \rangle_0 \\
&+ \langle \mathcal{T}\hat{O}(t_1)\hat{O}(t_3) \rangle_0 \langle \mathcal{T}\hat{O}(t_2)\ldots\hat{O}(t_{n-1})\hat{O}(t_n) \rangle_0 \\
&+ \ldots + \langle \mathcal{T}\hat{O}(t_1)\hat{O}(t_n) \rangle_0 \langle \mathcal{T}\hat{O}(t_2)\ldots\hat{O}(t_{n-1}) \rangle_0 \, , \qquad (2.13)
\end{aligned}$$

to represent higher-order correlators in terms of two-time correlators. To obtain an overview of the occurring terms, diagrammatic rules are introduced to represent terms with diagrams. Two-time correlators of operator $\hat{O}$ are represented by a straight line and correlators of $\hat{X}$ are represented by a sinusoidal line. The vertices, where lines are connected, represent points in time. Internal vertices involve an integration over time.

For example a diagram of the form

$$\text{———}\mathord{\curvearrowright\!\!\curvearrowright}\text{———} \tag{2.14}$$

represents terms like

$$\int\limits_{-\infty}^{\infty} \mathrm{d}t_a \int\limits_{-\infty}^{\infty} \mathrm{d}t_b \, \langle \mathcal{T}\hat{O}(t_1)\hat{O}(t_a)\rangle_0 \, \langle \mathcal{T}\hat{X}(t_a)\hat{X}(t_b)\rangle_0 \, \langle \mathcal{T}\hat{O}(t_b)\hat{O}(t_2)\rangle_0 \, . \tag{2.15}$$

While representing terms with diagrams, it is important to keep track of how often such kinds of terms appear in the equation.

In $\langle \mathcal{T}\mathcal{U}(\infty)\hat{O}(t)\hat{O}(0)\rangle_0$ a lot of different diagrams appear. Including terms where a diagram like the above is multiplied with a 'ring-like' structure consisting only of internal vertices. These kinds of terms are called disconnected diagrams. In standard diagrammatics, they are canceled by $\langle \mathcal{U}(\infty)\rangle_0$, which are called vacuum diagrams. The vacuum diagrams contain all possible diagrams without external vertices. That the vacuum diagrams cancel all disconnected diagrams in the context of the diagrammatics presented in this section is shown explicitly in Appendix A. The diagrammatics introduced here is the basis for the work presented in chapter 5.

3. Density matrix of a perturbed analog quantum simulator

The density matrix captures the information about the state of an open system and can be used to calculate, e.g., expectation values. In this chapter, we study the properties of the reduced density matrix of a perturbed system to understand the impact of the perturbation on the properties of the system. The perturbed system is assumed to be coupled weakly to a further bath that leads to relaxation to thermal equilibrium. The results can be used to understand the influence of additional degrees of freedom on an analog quantum simulator in thermal equilibrium. In previous work an equation of motion for the reduced density matrix has been derived using an expansion in the coupling Hamiltonian [46] and its properties were analyzed using a transformation to Laplace space. We found, that the impact of the perturbation, on one hand, is a renormalization of the energies. On the other hand, we studied under which condition a change of the eigenbasis occurs. The derivation of this equation is recapitulated at the beginning of this chapter. Beyond that, we present a solution of the equation of motion in Laplace space that leads to a general expression for the reduced density matrix depending on the bath self energy. With this, it is possible to study the influence of the environmental degrees of freedom on the eigenbasis of the system explicitly. As an example, we discuss the influence of bosonic degrees of freedom on a six qubit system. Herewith, we show that the external degrees of freedom can have a significant influence on the state of the

simulator and, hence, on its reliability. The work presented in this chapter is based on the publication [VI].

3.1. Introduction

In this chapter, we consider an analog quantum simulator in thermal equilibrium as shown in Fig. 2.2. The Hamiltonian of the simulator H_S is coupled to the external degrees of freedom (H_B) via H_C,

$$H = H_S + \lambda_B H_C + H_B \,, \tag{3.1}$$

with $\lambda_B = 1$. We state the theory in case of a simple coupling Hamiltonian. The system is coupled via operator $\hat{O}$ to bosonic modes of frequency ω_j with creation and annihilation operators $b_j^{(\dagger)}$,

$$H_C = \hat{O}\hat{X}, \qquad \text{with} \quad \hat{X} = \sum_j q_j = \sum_j t_j (b_j^\dagger + b_j) \,. \tag{3.2}$$

A generalization is the issue of Sec. 3.2.2.

We are interested in the influence of the external degrees of freedom on the density matrix of the simulator to study the reliability of analog quantum simulations. Without coupling to external degrees of freedom the density matrix is the equilibrium density matrix of the Hamiltonian describing the simulator, $\rho_S = e^{-\beta H_S}/\text{Tr}(e^{-\beta H_S})$. Using a diagrammatic technique we calculate the reduced density matrix of the simulator $\tilde{\rho}_S = \text{Tr}_B(\rho)$, with $\rho = e^{-\beta H}/\text{Tr}(e^{-\beta H})$, to compare it with ρ_S. With this, we study the reliability of analog quantum simulators or adiabatic quantum computations in thermal equilibrium. Perturbations in adiabatic quantum computations have already been examined [47–49]. The reduced density matrix of classical and quantum systems has been analyzed using similar approaches to this work [30, 36].

The diagrammatic expansion for $\tilde{\rho}_S$ presented in Ref. [46] is outlined in Sec. 3.2. The result of this expansion is an equation of motion for the reduced density matrix. In Sec. 3.3 we solve this equation in Laplace space. Lowest order results are examined in Sec. 3.4. Exemplary, we apply this results to a six qubit system.

3.2. Diagrammatic expansion

Using a transformation to the interaction picture with

$$S_0(\tau) = e^{-\tau(H_S + H_B)} \tag{3.3}$$

we define the time evolution operator in the interaction picture

$$\mathcal{S}(\tau) = \mathcal{T} \exp \left(- \int_0^\tau d\tau' \, H_{C,I}(\tau') \right) . \tag{3.4}$$

The reduced density matrix can be expressed using this time evolution operator.

$$
\begin{aligned}
\tilde{\rho}_S &= \mathrm{Tr}_B \left(\frac{1}{\mathrm{Tr}(e^{-\beta H})} e^{-\beta H} \right) \\
&= \mathrm{Tr}_B \left(\frac{1}{\mathrm{Tr}(e^{-\beta H})} e^{-\beta(H_S + H_B)} \cdot \mathcal{S}(\beta) \right) .
\end{aligned} \tag{3.5}
$$

A similar approach based on the introduction of $\mathcal{S}(\beta)$ has been presented by Deng et al. [30]. In contrast to our work, they perform a perturbation expansion in lowest order in H_C. Introducing the partition function $Z = \mathrm{Tr}(e^{-\beta H})$, and the partition functions of system Z_S and bath Z_B accordingly, the reduced density matrix is given by,

$$\tilde{\rho}_S = \rho_S \frac{Z_S Z_B}{Z} \, \mathrm{Tr}_B \left(\rho_B \mathcal{S}(\beta) \right) . \tag{3.6}$$

With this, we have an expression for the reduced density matrix of the perturbed system in terms of the density matrix ρ_S of the ideal system ($\lambda_B = 0$). The influence of the coupling to the external degrees of freedom is captured by the bath expectation value of $\mathcal{S}(\beta)$. The ideal expectation value of $\mathcal{S}(\beta)$ are the so-called vacuum diagrams $\langle \mathcal{S}(\beta) \rangle_0$. They correspond to the fraction of partition functions,

$$\langle \mathcal{S}(\beta) \rangle_0 = \text{Tr}\left(\rho_S \rho_B \mathcal{S}(\beta) \right) = \frac{Z}{Z_S Z_B} \ . \tag{3.7}$$

Herewith, the reduced density matrix only depends on two quantities, the ideal density matrix and expectation values of the time evolution operator of the coupling Hamiltonian,

$$\tilde{\rho}_S = \frac{1}{\langle \mathcal{S}(\beta) \rangle_0} \, \rho_S \, \langle \mathcal{S}(\beta) \rangle_B \ . \tag{3.8}$$

We study the properties of this reduced density matrix approximately using an expansion of the time evolution operator $\mathcal{S}(\beta)$ in orders of the coupling Hamiltonian,

$$\mathcal{S}(\beta) \approx 1 - \underbrace{\int_0^\beta H_C(\tau) \mathrm{d}\tau}_{Tr_B \Rightarrow 0} + \int_0^\beta \mathrm{d}\tau_1 \int_0^{\tau_1} \mathrm{d}\tau_2 H_C(\tau_1) H_C(\tau_2) + \ldots \ . \tag{3.9}$$

In the expectation value contributions only arise from terms of even order in the coupling Hamiltonian. $\langle H_C \rangle_B = 0$ holds because a fitting constant can always be added to the Hamiltonian.

Looking at the expansion for one matrix element of the reduced density matrix allows us to define diagrammatic rules. With diagrammatic techniques it is possible to study higher order terms. We denote the eigenstates and eigenenergies of the system by

$$H_S \left| s \right\rangle = E_s \left| s \right\rangle \ . \tag{3.10}$$

With this, the lowest order terms for the expansion of a matrix element reads,

$$\langle s'|\tilde{\rho}_S|s\rangle \approx \frac{1}{Z_S \langle \mathcal{S}(\beta)\rangle_0} e^{-(\beta-0)E_{s'}} \delta_{s,s'}$$

$$+\frac{1}{Z_S \langle \mathcal{S}(\beta)\rangle_0} \int\limits_0^\beta \mathrm{d}\tau_1 \int\limits_0^{\tau_1} \mathrm{d}\tau_2 \sum_{\bar{s},j} e^{-(\beta-\tau_1)E_{s'}} \langle s'|\hat{O}|\bar{s}\rangle$$

$$\cdot\, e^{-(\tau_1-\tau_2)E_{\bar{s}}} \langle \bar{s}|\hat{O}|s\rangle\, e^{-(\tau_2-0)E_s} \langle q_j(\tau_1)q_j(\tau_2)\rangle_B$$

$$+\mathcal{O}(H_C^4)\,, \tag{3.11}$$

where we assume bath modes to be independent, $\langle q_j(\tau_1)q_k(\tau_2)\rangle = 0$ for $j \neq k$.

The prefactor $^1/_{Z_S \langle \mathcal{S}(\beta)\rangle_0}$ is not included in the diagrammatic calculations since the resulting density matrix can be normalized afterward. Therefore, we introduce the unnormalized reduced density matrix $\tilde{\rho}_S^{(u)}$,

$$\tilde{\rho}_S^{(u)} = Z_S \langle S\rangle_0 \tilde{\rho}_S\,. \tag{3.12}$$

In a diagram the imaginary time runs form right to left. Usually, a diagram starts at $\tau = 0$ and ends on the left with β. We use a bold straight line as the diagrammatic representation for $\tilde{\rho}_S^{(u)}$. Straight lines are used to picture free propagations $e^{-(\tau_{left}-\tau_{right})H_S}$. A dashed line indicates a bath correlator $\sum_j \langle q_j(\tau_{left})q_j(\tau_{right})\rangle_B$ and corresponds to two operators $\hat{O}$. The diagram depicts the order of all operators. One of the two operators $\hat{O}$ is placed at each end of the dashed line. Every full vertex, where straight lines and dashed lines come together, is associated with an integration of τ_n, $\int_0^{\tau_{n-1}} \mathrm{d}\tau_n$, where τ_n is varied between zero and the time τ_{n-1} left of τ_n. With this integrals, the time-ordering in Eq. (3.9) is given implicitly. In the case of a diagram that does not start at $\tau = 0$, the limits of integration have to be chosen accordingly.

Using these diagrammatic rules, the expansion for the unnormalized reduced density

matrix (cf. Eq. (3.11)) is depicted by

$$\tag{3.13}$$

Higher order diagrams can be summed up using a Dyson equation

$$\tag{3.14}$$

where the self energy is given by

$$\tag{3.15}$$

The Dyson equation reads

$$\tilde{\rho}_S^{(u)}(\beta) = e^{-\beta H_S} + \int\limits_0^\beta \mathrm{d}\tau_1 \int\limits_0^{\tau_1} \mathrm{d}\tau_2\, e^{-(\beta-\tau_1)H_S} \Sigma(\tau_1 - \tau_2)\tilde{\rho}_S^{(u)}(\tau_2)\,, \tag{3.16}$$

where the self energy in lowest order is given by

$$\Sigma^{(1)}(\tau_l - \tau_r) = \sum_{\bar{s},j} \hat{O} \ket{\bar{s}}\, e^{-(\tau_l - \tau_r)E_{\bar{s}}} \bra{\bar{s}} \hat{O} \braket{q_j(\tau_l)q_j(\tau_r)}_B\,. \tag{3.17}$$

Introducing the spectral density $S(\omega)$ of the bath modes,

$$\sum_j \braket{q_j(\tau_1)q_j(\tau_2)}_B = \int \frac{\mathrm{d}\omega}{2\pi} S(\omega) e^{-\omega(\tau_1 - \tau_2)}\,, \tag{3.18}$$

the self energy reads

$$\Sigma^{(1)}(\tau_l - \tau_r) = \int \frac{d\omega}{2\pi} \sum_{\bar{s}} \hat{O} |\bar{s}\rangle \, e^{-(\tau_l - \tau_r)E_{\bar{s}}} \langle \bar{s}| \, \hat{O} \, S(\omega) e^{-\omega(\tau_l - \tau_r)} \, . \tag{3.19}$$

The derivative of Eq. (3.16) with respect to β yields an equation of motion for the unnormalized reduced density matrix

$$\frac{\partial}{\partial \beta} \tilde{\rho}_S^{(u)}(\beta) = -H_S \tilde{\rho}_S^{(u)}(\beta) + \int\limits_0^\beta d\tau_2 \, \Sigma(\beta - \tau_2) \tilde{\rho}_S^{(u)}(\tau_2) \, . \tag{3.20}$$

This equation resembles the well-known master equation. In this case, time is replaced by the inverse temperature β. Furthermore, the self energy is not a superoperator. Solving Eq. (3.20) and normalizing with

$$\mathrm{Tr}_S \, \tilde{\rho}_S = 1 \, , \tag{3.21}$$

results in an approximation for the reduced density matrix $\tilde{\rho}_S$.

3.2.1. Truncation of the series for $\tilde{\rho}_S^{(u)}$

In [46] the truncation of the series for the self energy is examined. However, we present here the numerical investigation of the convergence of the series for the reduced density matrix and for the self energy as presented in Ref. [VI]. For this purpose, we focus on the diagrams of first and second order in H_C,

$$\text{I:} \quad \tag{3.22}$$

To study the behavior of the diagrams we set the matrix elements of $\hat{O}$ and the exponential function of the free propagations to unity and focus on the limit $\beta \to \infty$. The resulting dominating terms are the following,

$$\text{I} \propto \int \frac{d\omega_1}{2\pi} \, \beta \frac{S(\omega_1)}{\omega_1} \tag{3.23}$$

$$\text{II} \propto \iint \frac{d\omega_1}{2\pi} \frac{d\omega_2}{2\pi} \, \beta \frac{S(\omega_1)S(\omega_2)}{\omega_1^2\omega_2 + \omega_1\omega_2^2} \tag{3.24}$$

$$\text{III} \propto \iint \frac{d\omega_1}{2\pi} \frac{d\omega_2}{2\pi} \, \beta^2 \frac{S(\omega_1)S(\omega_2)}{2\omega_1\omega_2} \, . \tag{3.25}$$

We consider an ohmic spectrum with Lorentzian cutoff at frequency ω_c,

$$S(\omega) = \frac{\eta\omega}{(1 - e^{-\beta\omega})(1 + (\omega/\omega_c)^2)} \, , \tag{3.26}$$

with coupling strength η. Introducing the dimensionless parameter $\nu_{1/2} = {}^{\omega}/{}_{\omega_c}$, and the dimensionless spectral density $\tilde{S}(\nu) = {}^{S(\nu\omega_c)}/{}_{\eta\omega_c}$, the behavior of the diagrams reads,

$$\text{I} \propto \eta\beta\omega_c \int \frac{d\nu_1}{2\pi} \frac{\tilde{S}(\nu_1)}{\nu_1} \tag{3.27}$$

$$\text{II} \propto \eta^2\beta\omega_c \iint \frac{d\nu_1}{2\pi} \frac{d\nu_2}{2\pi} \frac{\tilde{S}(\nu_1)\tilde{S}(\nu_2)}{\nu_1^2\nu_2 + \nu_1\nu_2^2} \tag{3.28}$$

$$\text{III} \propto \eta^2\beta^2\omega_c^2 \iint \frac{d\nu_1}{2\pi} \frac{d\nu_2}{2\pi} \frac{\tilde{S}(\nu_1)\tilde{S}(\nu_2)}{2\nu_1\nu_2} \, . \tag{3.29}$$

Fig. 3.1 displays a numerical calculation for diagrams II and III, where we consider all orders in β. For $\eta \ll 1$ diagram II is neglectable in comparison to the first order diagram I. Whereas, the separable diagram III is only neglectable to I if,

$$\eta\beta\omega_c \ll 1 \, . \tag{3.30}$$

This shows that non-separable diagrams can be neglected. However, it is necessary, to sum up separable diagrams within the self energy, especially in the limit $\beta \to \infty$.
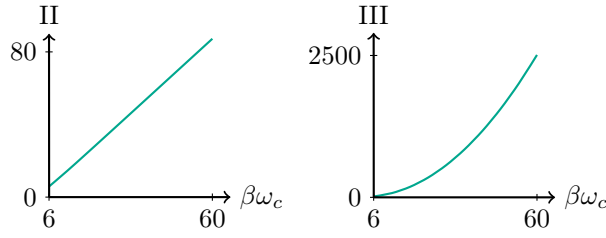
Figure 3.1.: The graphs show the β dependence of diagrams II and III (for $\eta = 1$). Reprinted with permission of Ref. [VI]. Copyright (2016) by the American Physical Society.

The similarity of the diagrams of the self energy to the diagrams of the reduced density matrix allows us to transfer the results to this case. With this, we see,

$$\left(\sum\right) = \underset{\propto \text{I}}{\bigcap} + \underset{\propto \text{II}}{\bigcap\bigcap} + \underset{\propto \text{II}}{\bigcap\bigcap} + \cdots \quad , \tag{3.31}$$

that a truncation of the series for the self energy for $\eta < 1$ is justified.

3.2.2. Generalization of H_C

As indicated in Sec. 2.1 it is possible to generalize the coupling Hamiltonian, used to derive the equation of motion for the reduced density matrix, to a more realistic case. Each element of the simulator, e.g. qubits or resonators, could be coupled to an individual bath,

$$H_C = \sum_{i=1}^{N} \hat{O}^i \hat{X}^i = \sum_i h_i \qquad \text{with} \qquad \hat{X}^i = \sum_j q_j^{(i)} \,, \tag{3.32}$$

where the baths are independent

$$\langle q_j^{(i)}(\tau_1) q_j^{(k)}(\tau_2) \rangle_B = 0 \quad \text{for} \quad i \neq k \,. \tag{3.33}$$

If the properties of the baths are identical,

$$\langle q_j^{(i)}(\tau_1) q_j^{(i)}(\tau_2) \rangle_B = \langle q_j^{(k)}(\tau_1) q_j^{(k)}(\tau_2) \rangle_B \,, \tag{3.34}$$

the lowest order of the self energy is formed by the sum of the self energies for coupling operators h_i,

$$\Sigma^{(1)} = \sum_i \Sigma_i^{(1)} \,, \tag{3.35}$$

as outlined in Ref. [46].

For the diagrammatic expansion, we assumed the bath modes to be bosonic. In the case of superconducting qubits, fermionic perturbations are possible [34, 35], which could also be covered by this theory. Under the assumption that only equivalent pairs of annihilation and creation operators are chosen [50], the results of this work directly apply using the spectral function of the bath as given in Eq. (20) in Ref. [51]. To consider a fermionic bath in more generality, the contraction rules for the bath correlators have to take into account the appropriate sign change [52].

3.3. General solution

Solving Eq. (3.20) results in an approximation for the reduced density matrix of the perturbed quantum simulator. This equation of motion for the reduced density matrix appears to have some similarity to master equations. Lowest order results are usually obtained within the Markov approximation in standard master equation calculations [53]. In case of an ohmic spectral density, the bath correlator in imaginary time is not an

exponentially decaying function. Since it has peaks at $\tau = 0$ and $\tau = \beta$, a Markov approximation is not applicable. Therefore, we solve the equation in Laplace space to study the lowest order results. The convolution integral in Eq. (3.20) indicates a transformation to Laplace space with

$$\tilde{\rho}_S^{(u)}(\epsilon) = \int\limits_0^\infty \tilde{\rho}_S^{(u)}(\tau)\, e^{-\epsilon\tau}\, \mathrm{d}\tau \text{ , with } \epsilon \in \mathbb{C}\,. \tag{3.36}$$

The equation of motion for the unnormalized reduced density matrix (Eq. (3.20)) transforms to

$$\epsilon\tilde{\rho}_S^{(u)}(\epsilon) - \tilde{\rho}_S^{(u)}(\tau = 0) = (-H_S + \Sigma(\epsilon))\,\tilde{\rho}_S^{(u)}(\epsilon)\,. \tag{3.37}$$

With this, the unnormalized reduced density matrix is given by

$$\tilde{\rho}_S^{(u)}(\epsilon) = (\epsilon + H_S - \Sigma(\epsilon))^{-1}\,\tilde{\rho}_S^{(u)}(\tau = 0)\,. \tag{3.38}$$

Since the imaginary time τ represents the inverse temperature, $\tau = 0$ corresponds to an infinitely high temperature. Therefore, the assumption $\tilde{\rho}_S^{(u)}(\tau = 0) \propto \mathbb{1}$ is justified. A physically reasonable solution for the reduced density matrix has to be hermitian. For the density matrix in Laplace space this means

$$\left(\tilde{\rho}_S^{(u)}(\epsilon)\right)^\dagger = \tilde{\rho}_S^{(u)}(\epsilon^*)\,. \tag{3.39}$$

In order to fulfill this condition with Eq. (3.38) we find the following requirements

$$1)\quad \Sigma^\dagger(\epsilon) = \Sigma(\epsilon^*) \Rightarrow \Sigma^\dagger(\tau) = \Sigma(\tau) \tag{3.40}$$

$$2)\quad [\tilde{\rho}_S^{(u)}(\epsilon), -H_S + \Sigma(\epsilon)] = 0\,. \tag{3.41}$$

The first requirement is achieved, since the full self energy is hermitian. With the assumption $\tilde{\rho}_S^{(u)}(\tau = 0) \propto \mathbb{1}$ the second requirement is also fulfilled.

Eq. (3.38) was derived and analyzed in Ref. [46]. Beyond this, we present the calculation of the inverse Laplace transform to find the reduced density matrix $\tilde{\rho}_S^{(u)}$ as presented in Ref. [VI] using the residue theorem. The inverse Laplace transform reads

$$\tilde{\rho}_S^{(u)}(\tau) = \frac{1}{2\pi i} \int_{\kappa-i\infty}^{\kappa+i\infty} \tilde{\rho}_S^{(u)}(\epsilon)\, e^{\epsilon\tau}\, \mathrm{d}\epsilon \,. \tag{3.42}$$

With the residue theorem a calculation of this integral is possible, where $\kappa \in \mathbb{R}$ is in the region of convergence of $\tilde{\rho}_S^{(u)}(\epsilon)$. The integration contour is closed counterclockwise with a semicircle with infinite radius. The additional integration path gives no contribution since the reduced density matrix can be approximated with a rational function on this contour. With this, all singularities of $\tilde{\rho}_S^{(u)}(\epsilon)$ are enclosed. The reduced density matrix is given by a sum over all isolated singularities i,

$$\tilde{\rho}_S^{(u)}(\tau) = \sum_i \mathrm{Res}_i \left(e^{\tau\epsilon} \tilde{\rho}_S^{(u)}(\epsilon) \right) . \tag{3.43}$$

The reduced density matrix in Laplace space is given by the inverse of $\epsilon + H_S - \Sigma(\epsilon)$. Writing the inverse matrix with determinant and adjugate matrix

$$\tilde{\rho}_S^{(u)}(\epsilon) = \frac{1}{\det\left(\epsilon + H_S - \Sigma(\epsilon)\right)} \, \mathrm{adj}\left(\epsilon + H_S - \Sigma(\epsilon)\right), \tag{3.44}$$

allows us to identify the singularities. On one hand, the roots of the determinate are singularities of $\tilde{\rho}_S^{(u)}(\epsilon)$. On the other hand, the adjugate matrix has singularities at the singularities of the self energy $\Sigma(\epsilon)$, since the components of the adjugate matrix are multiplications of $\epsilon + H_S - \Sigma(\epsilon)$. The latter are canceled because they also appear in the determinant. Therefore, only the roots of the determinant contribute in Eq. (3.43). Assuming these singularities to be simple poles, the reduced density matrix reads

$$\tilde{\rho}_S^{(u)}(\tau) = \sum_i e^{-\tau E_i^{re}} \frac{\mathrm{adj}\left(-E_i^{re} + H_S - \Sigma(-E_i^{re})\right)}{\prod_{j\neq i}(E_j^{re} - E_i^{re})} \,, \tag{3.45}$$

where the renormalized energies E_i^{re} are the roots of the determinant. For small self energy, so in the limit of small effect of the external degrees of freedom, the roots of the determinant are approximately given by

$$\epsilon_s = -E_s + \Sigma_{ss}(-E_s), \qquad (3.46)$$

so that the renormalized energy is $E_s^{re} = E_s - \Sigma_{ss}(-E_s)$. The renormalized energies can also be determined by numerical calculations. For larger coupling to the external degrees of freedom, where the self energy has a significant dependence on the energy, the determinant may have more roots than the dimension of H_S.

In comparison to an equilibrium density matrix, we recognize that the exponential factors remain, but with renormalized energies,

$$(\tilde{\rho}_S(\beta))_{ss'} = \sum_n f_n^{ss'}(\beta) e^{-\beta E_n^{re}} . \qquad (3.47)$$

The factors $f_n^{ss'}(\beta)$ describe the change of the eigenbasis depending on the coupling strength η. For $\eta \to 0$ the matrix will be diagonal in the eigenbasis of H_S, but for infinite coupling strength, the density matrix will commute with H_C [37, 38]. Calculating the self energy for specific model systems, it is possible to study the influence of external degrees of freedom by analyzing Eq. (3.45).

In case of an arbitrary two dimensional system with non-degenerate eigenenergies we can write down the reduced density matrix explicitly,

$$\begin{aligned}
\tilde{\rho}_S^{(u)}(\beta) \propto{}& e^{-\beta E_1^{re}} \cdot \begin{pmatrix} E_2 - E_1^{re} - \Sigma_{22}(-E_1^{re}) & \Sigma_{21}(-E_1^{re}) \\ \Sigma_{12}(-E_1^{re}) & E_1 - E_1^{re} - \Sigma_{11}(-E_1^{re}) \end{pmatrix} \\
&- e^{-\beta E_2^{re}} \cdot \begin{pmatrix} E_2 - E_2^{re} - \Sigma_{22}(-E_2^{re}) & \Sigma_{21}(-E_2^{re}) \\ \Sigma_{12}(-E_2^{re}) & E_1 - E_2^{re} - \Sigma_{11}(-E_2^{re}) \end{pmatrix} .
\end{aligned} \qquad (3.48)$$

This illustrates the renormalization of the energies and the change of the eigenbasis depending on the self energy.

3.4. Lowest order results

The expression for the reduced density matrix (Eq. (3.45)) depends on the self energy in Laplace space. In this section, we analyze this equation in lowest order of the self energy, so we truncate the series for the self energy after the first term,

$$\Sigma^{(1)}(\epsilon) = \int \frac{d\omega}{2\pi} \sum_{\bar{s}} \hat{O} \, |\bar{s}\rangle \, \langle \bar{s}| \, \hat{O} \frac{S(\omega)}{E_{\bar{s}} + \epsilon + \omega} \,. \tag{3.49}$$

This expression is the analytical continuation of the result for $\mathrm{Re}(E_{\bar{s}} + \epsilon + \omega) > 0$. Since this term is hermitian the condition for a hermitian density matrix (Eq. (3.40)) is satisfied. We will assume an ohmic spectral density with Lorentzian cutoff ω_c and coupling strength η (Eq. (3.26)).

To calculate the self energy in lowest order, the following integral has to be evaluated,

$$I(E_s, \epsilon) = \int\limits_{-\infty}^{+\infty} \frac{d\omega}{2\pi} \frac{1}{E_s + \epsilon + \omega} \frac{\omega}{1 - e^{-\beta\omega}} \frac{\eta}{1 + (\omega/\omega_c)^2} \,. \tag{3.50}$$

Using the residue theorem, we find

$$\begin{aligned}
I(E_s) = &- i \frac{\epsilon + E_s}{1 - e^{\beta(\epsilon + E_s)}} \frac{\eta}{1 + (\epsilon + E_s)^2/\omega_c^2} \Theta_{1/2}\big(-\mathrm{Im}(\epsilon)\big) \\
&+ i \frac{\omega_c^2 \eta}{2} \frac{1}{E_s + \epsilon + i\omega_c} \frac{1}{1 - e^{-i\beta\omega_c}} - \sum_{n=1}^{\infty} \frac{\nu_n \eta}{\beta} \frac{1}{E_s + \epsilon + i\nu_n} \frac{1}{1 - (\nu_n/\omega_c)^2} \,,
\end{aligned} \tag{3.51}$$

where $\omega_c \neq \nu_n$ and $\epsilon \notin \{-E_s - i\omega_c, -E_s - i\nu_n\}$ with $n \in \mathbb{N}$ and the Matusbara frequencies $\nu_n = 2\pi n/\beta$. We have introduced $\Theta_{1/2}(x)$, which represents the the step function, with value $1/2$ at $x = 0$.

Using the appropriate operator $\hat{O}$ we can evaluate $\Sigma^{(1)}(\epsilon)$ and with this calculate $\tilde{\rho}_S^{(u)}(\beta)$ according to Eq. (3.45). In the following subsections, we apply this to two qubit model systems. On one hand, we study the influence of external degrees of freedom on a measurable quantity, in this case, an equilibrium expectation value. On the other hand, we illustrate the influence of external degrees of freedom on specific matrix elements of the density matrix. With this, we show that key quantum properties, such as entanglement and coherence, can be affected by the external degrees of freedom even in thermal equilibrium.

3.4.1. Model system - one qubit

We examine a toy model of a two-level system disturbed by a bosonic environment

$$H_S = \frac{1}{2}\Delta E\, \sigma_z \quad H_B = \sum_i \omega_i b_i^\dagger b_i \quad \hat{O} = \sigma_x + \sigma_z\,, \tag{3.52}$$

to illustrate the influence of external degrees of freedom on measurable quantities. The first-order self energy is a two by two matrix,

$$\Sigma^{(1)}(\epsilon) = \begin{pmatrix} I(-\Delta E/2, \epsilon) + I(\Delta E/2, \epsilon) & -I(-\Delta E/2, \epsilon) + I(\Delta E/2, \epsilon) \\ -I(-\Delta E/2, \epsilon) + I(\Delta E/2, \epsilon) & I(-\Delta E/2, \epsilon) + I(\Delta E/2, \epsilon) \end{pmatrix}\,. \tag{3.53}$$

Evaluating $I(\Delta E/2, \epsilon)$ with Eq. (3.51) allows us to calculate the reduced density matrix of the perturbed system with Eq. (3.48). Fig. 3.2 displays the equilibrium expectation value of σ_x. It decreases with increasing coupling strength η. With this, we see that in thermal equilibrium external degrees of freedom can affect the state of the system so that measurable quantities change significantly.
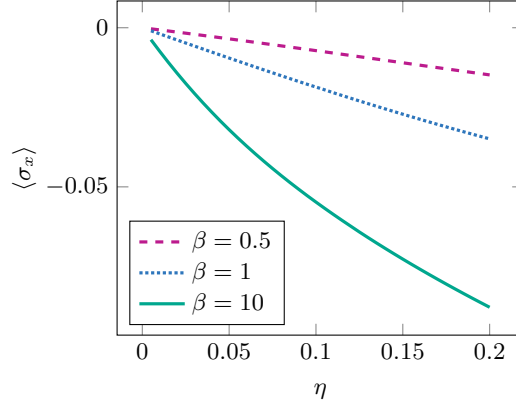
Figure 3.2.: The expectation value of σ_x is plotted as a function of the coupling strength η. Values of further parameters are $\Delta E = 1$, $\omega_c = 10$. Reprinted with permission of Ref. [VI]. Copyright (2016) by the American Physical Society.
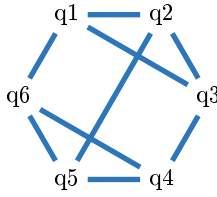
Figure 3.3.: This sketch indicates the qubit pairs with non-zero Ising interaction. Reprinted with permission of Ref. [VI]. Copyright (2016) by the American Physical Society.

3.4.2. Model system - six qubits

Now we focus on a more complex model system of six qubits. It is similar to the eight qubit unit cell of the quantum annealing processor presented by Lanting et al. [54],

$$H_S = \epsilon \sum_{i<j} J_{ij}\, \xi_1^{(i,j)} \sigma_z^{(i)} \sigma_z^{(j)} - \frac{1}{2}\Delta \sum_i \xi_2^{(i)} \sigma_x^{(i)} \,. \tag{3.54}$$

The Ising interaction J_{ij} is present for some qubit pairs as indicated in Fig. 3.3. We

introduce Gaussian random numbers $\xi_{1/2}$ with mean value 1 to avoid degeneracy. Otherwise, this would complicate the calculation of residues, and Eq. (3.45) could not be used.

All qubits are coupled to individual, but identical bosonic baths (Eqs. (3.33), (3.34)) with an ohmic spectral density (Eq. (3.26)),

$$H_B = \sum_{i,k} \omega_k \, b_k^{\dagger(i)} b_k^{(i)} \quad H_C = \sum_i \sigma_z^{(i)} \sum_k f_k^{(i)} (b_k^{\dagger(i)} + b_k^{(i)}) \,. \tag{3.55}$$

We derived the equation for the reduced density matrix based on a simple coupling Hamiltonian. In section 3.2.2, we showed how the results can be generalized to this kind of coupling Hamiltonian. To perform the numerical simulation for the reduced density matrix it is necessary to calculate the adjugate matrix. A significant improvement for this calculation can be obtained by using matrix decompositions [55].

The ground state of the six-qubit system described by H_S is, for the chosen set of parameters, approximately the highly entangled Greenberger-Horne-Zeilinger (GHZ) state [56] of six qubits

$$|\psi_o\rangle \approx \frac{1}{\sqrt{2}} \left(|\uparrow\uparrow \ldots\rangle + |\downarrow\downarrow \ldots\rangle \right) \,. \tag{3.56}$$

The entanglement of this state is expressed by matrix element $\langle \uparrow\uparrow \ldots | \rho_{GHZ} | \downarrow\downarrow \ldots \rangle$ of the density matrix. We study this matrix element, depending on the coupling strength η, to show that external degrees of freedom can reduce the entanglement. The results are shown in Fig. 3.4. We see that the matrix element is smaller for higher temperatures. This is due to the fact, that with increasing temperature a state similar to $\frac{1}{\sqrt{2}} \left(|\uparrow\uparrow \ldots\rangle - |\downarrow\downarrow \ldots\rangle \right)$ gets populated. Since each qubit is coupled individually to external degrees of freedom via $\sigma_z^{(i)}$, the density matrices of the qubits will be diagonal in the eigenbasis of $\sigma_z^{(i)}$ when the coupling is infinitely large. So with increasing η, the reduced density matrix will advance toward a product state. This is the reason for the decay of
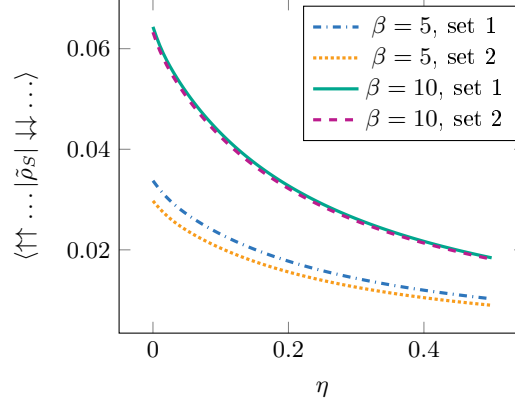
Figure 3.4.: We show the matrix element $\langle \uparrow\uparrow \ldots |\tilde{\rho}_S| \downarrow\downarrow \ldots\rangle$ as function of the coupling strength η. The matrix element decreases strongly with increasing η. This graph displays exemplary results for two sets of random variables $\xi_1^{(i,j)}$, $\xi_2^{(i)}$ (Gaussian random numbers with mean value 1 and variance 0.2 / 0.1) for two temperatures. Further parameters are $\epsilon = 0.5$; $\Delta = 3$; $\omega_c = 15$; $J_{ij} = -3.01$ for the connections shown in Fig. 3.3, otherwise $J_{ij} = 0$. Reprinted with permission of Ref. [VI]. Copyright (2016) by the American Physical Society.

the matrix element $\langle \uparrow\uparrow \ldots |\tilde{\rho}_S| \downarrow\downarrow \ldots\rangle$. So the coupling to external degrees of freedom results in a decreasing quantum coherence.

4. Estimating the error of a perturbed analog quantum simulator by additional measurements

The reliability of a quantum simulator is a fundamental obstacle on the way to useful simulations. In this chapter, we present a possibility to determine on which timescale a quantum simulation is reliable. We study a quantum system in presence of external degrees of freedom with a known spectral density. These environmental degrees of freedom cause a perturbation of the quantum system that builds the simulator. With advancing time the influence of the external degrees of freedom on the state of the system, and hence on the result of the simulation, is expected to increase. Since an interesting quantum problem cannot be simulated or verified by classical computations, it is challenging to find out whether the influence of the external degrees of freedom substantially alters the state of the simulator. Without a possibility to verify the results, quantum simulation cannot be used to solve problems that are classically intractable. We study the effect of perturbations on the result of the simulation in lowest order. This allows us to derive a simple protocol to verify the reliability of a quantum simulator that is subject to small noise. This method is based on additional measurements on the simulator. Here, we assume the result of the simulation to be a time-dependent expectation value. As an example, we consider a two-level system coupled to a bosonic environment. This work had been presented before in Ref. [V].

4.1. Introduction

In this chapter, we study a perturbed analog quantum simulator as illustrated in Fig. 2.1. Though, we allow the system Hamiltonian H_S, which describes the quantum simulator, to be time dependent,

$$H(t) = H_S(t) + H_B + \lambda_B H_C \,, \tag{4.1}$$

where $\lambda_B = 1$ describes the full system with coupling via operator $\hat{O}$ ($H_C = \hat{O}\hat{X}$) to the environment described by H_B. The properties of the bath are described by the bath correlation function $\langle \hat{X}(t)\hat{X}(0)\rangle_0$, where $\hat{X}$ is an operator of the bath. The result of the simulation is an expectation value $\langle \hat{A}(t)\rangle_0$. Since the system Hamiltonian is time-dependent the case of digital quantum simulation, where a time-evolution is realized by applying gates, is also covered by this theory.

We perform a perturbation expansion of the expectation value on Keldysh contour [52] and focus on the lowest order (see Sec. 4.2). From this, we develop a protocol to estimate the effect of the perturbation on $\langle \hat{A}(t)\rangle_0$ and thereby the error in the simulation. This protocol is based on a self-consistent verification and requires additional measurements on the simulator, and knowledge of some properties of the bath. Since there are many possibilities to measure the bath correlator [42, 57], we assume a certain knowledge about the bath. The protocol is presented in Sec. 4.3. In Sec. 4.4 we give a simplified version of the self-consistent equation that demands only a rough knowledge of the bath. Our method is based on a consideration in lowest order of the coupling to the bath. In other works in the fields of quantum simulation and quantum computation, lowest order expansions are also used to cope with errors [24, 25]. Using our protocol, it is possible to determine the time-scale on which the error is small. This time-scales are discussed in Sec. 4.5. In Sec. 4.6 we apply our method to a toy model of a two-level system coupled to a bosonic bath. With this, we illustrate how the protocol verifies or rejects results of a simulation. Furthermore, we discuss the impact of higher order terms. To introduce

the protocol we use a simple coupling Hamiltonian. In Sec. 4.7 we discuss the case of multiple baths and also the case where the perturbation arises due to disorder in the system Hamiltonian.

4.2. Diagrammatic expansion

In this work, we study the influence of external degrees of freedom on the expectation value $\langle \hat{A}(t) \rangle_0$. The perturbed expectation value of operator $\hat{A}$ is given by,

$$
\begin{aligned}
\langle \hat{A}(t) \rangle &= \text{Tr}\left[\rho_0\, U_1(t_0, t)\, \hat{A}\, U_1(t, t_0) \right] \\
&= \text{Tr}\left[\rho_0 \mathcal{U}(t_0, t)\, \hat{A}_I(t) \mathcal{U}(t, t_0) \right] .
\end{aligned}
\tag{4.2}
$$

The time evolution operators are defined according to Sec. 2.3. With $U_1(t, t_0)$ we denote the time evolution of the full system,

$$
U_{\lambda_B}(t, t_0) = \mathcal{T} \exp\left(-i \int_{t_0}^{t} \mathrm{d}t'\, H(t') \right) ,
\tag{4.3}
$$

with time-ordering operator $\mathcal{T}$ ($t > t_0$). Whereas, $U_0(t, t_0)$ describes the time evolution of the ideal system. Index I denotes the interaction picture $\hat{B}_I(t) = U_0(t_0, t) \hat{B}\, U_0(t, t_0)$. And $\mathcal{U}(t, t_0)$ is the time evolution operator in the interaction picture,

$$
\mathcal{U}(t, t_0) = \mathcal{T} \exp\left(-i \int_{t_0}^{t} \mathrm{d}t'\, H_{C,I}(t') \right) .
\tag{4.4}
$$

We perform an expansion of Eq. (4.2) in orders of the coupling Hamiltonian H_C. An expansion on Keldysh contour (see Sec. 2.4) allows us to show the terms up to fourth

order in H_C,

$$\langle \hat{A}(t) \rangle = \quad + \quad + \quad + \quad + \quad + \quad + \quad + \quad +$$

$$+ \quad + \quad + \quad + \quad + \quad + \quad + \quad +$$

$$+ \quad + \quad + \quad + \quad + \ldots . \tag{4.5}$$

In this diagrams, straight lines denote the ideal time evolution (U_0), whereby the upper line represents the forward time evolution and the lower line the backward time evolution. Orders of H_C are pictured by the black dots, where we consider explicit time sorting. The position of operator $\hat{A}$ at time t is not displayed explicitly. Based on the assumption $\langle H_C \rangle = 0$, which is justified since appropriate terms can be added to the Hamiltonian, odd orders in H_C vanish. Zeroth order in H_C represents the ideal result $\mathrm{Tr}\left[\rho_0 \hat{A}_I(t)\right] = \langle \hat{A}(t) \rangle_0$, where the index 0 implies that the appropriate time evolution operator is $U_{\lambda_B=0}$. Up to second order we find,

$$\langle \hat{A}(t) \rangle \approx \mathrm{Tr}\left[\rho_0 \hat{A}_I(t)\right] + \int\limits_{t_0}^{t} dt_1 \int\limits_{t_0}^{t_1} dt_2 \, C_2(t, t_1, t_2), \tag{4.6}$$

The lowest-order correction $C_2(t, t_1, t_2)$ is given by

$$\begin{aligned}
C_2(t, t_1, t_2) = & \langle \hat{O}(t_1) \hat{A}(t) \hat{O}(t_2) \rangle_0 \, \langle \hat{X}(t_1) \hat{X}(t_2) \rangle_0 \\
& + \langle \hat{O}(t_2) \hat{A}(t) \hat{O}(t_1) \rangle_0 \, \langle \hat{X}(t_2) \hat{X}(t_1) \rangle_0 \\
& - \langle \hat{O}(t_2) \hat{O}(t_1) \hat{A}(t) \rangle_0 \, \langle \hat{X}(t_2) \hat{X}(t_1) \rangle_0 \\
& - \langle \hat{A}(t) \hat{O}(t_1) \hat{O}(t_2) \rangle_0 \, \langle \hat{X}(t_1) \hat{X}(t_2) \rangle_0 ,
\end{aligned} \tag{4.7}$$

in the case of the simple but general form of the coupling Hamiltonian $H_C = \hat{O}\hat{X}$. If the influence of the external degrees of freedom is perturbative, this lowest-order correction is a measure for the induced error.

4.3. Protocol to estimate errors

In this section, we explain how the lowest order correction C_2 can be used to estimate the error induced by the external degrees of freedom. To evaluate C_2 the noise correlator $\langle \hat{X}(t_1)\hat{X}(t_2)\rangle_0$ has to be known approximately. The noise correlator can be determined using calibration methods or by theoretical estimations.

We present a protocol to examine the difference between the measurement result $\langle \hat{A}(t)\rangle$ and the ideal value $\langle \hat{A}(t)\rangle_0$ in a self-consistent manner.

1. **Measurement:** The expectation value $\langle \hat{A}(t)\rangle$ and the three-time correlators like $\langle \hat{O}(t_1)\hat{A}(t)\hat{O}(t_2)\rangle$ that appear in Eq. (4.7) have to be measured. The result of this measurements are quantities of the perturbed system.

2. **Assume small perturbation:** Assuming that the perturbation is small allows us to use the measured quantities as ideal values $\langle \hat{A}(t)\rangle \approx \langle \hat{A}(t)\rangle_0$, $\langle \hat{O}(t_1)\hat{A}(t)\hat{O}(t_2)\rangle \approx \langle \hat{O}(t_1)\hat{A}(t)\hat{O}(t_2)\rangle_0$, etc.. This assumption will be verified self-consistently in the next step.

3. **Verify the assumption:** With this perturbed values we calculate C_2. If the assumptions in point 2 are valid the value of C_2 is small in comparison to the expectation value,

$$\left| \int_{t_0}^{t} \mathrm{d}t_1 \int_{t_0}^{t_1} \mathrm{d}t_2 \, C_2(t, t_1, t_2) \right| \ll \left| \langle \hat{A}(t)\rangle \right| . \tag{4.8}$$

In the case that Eq. (4.8) is fulfilled, the initial assumption was correct. This means, that the influence of the external degrees of freedom is actually small and the simulation is reliable. If Eq. (4.8) is not true, the assumptions in the second step of the protocol are not valid. Therefore, it is not possible to make a statement about the reliability of the simulator with this protocol.

As part of this protocol, it is necessary to measure correlators of three times of the form $\langle \hat{O}(t_1)\hat{A}(t)\hat{O}(t_2)\rangle$. With only one ancilla qubit it is possible to measure two-time correlators [58–60]. These techniques can be generalized to measure three-time correlators. In the next section, we describe a simplified version of the protocol that only requires the measurement of correlators of one time and less precise knowledge of the bath.

4.4. Simplified condition

Decoherence in quantum systems is usually described using the master equation approach. In this descriptions, the bath correlation functions are often represented by sums of exponential functions. When the effect of the bath is small it is possible to approximate the bath correlation function as a single exponential function,

$$\langle \hat{X}(t_1)\hat{X}(t_2)\rangle_0 \approx \lambda e^{-\gamma|t_1-t_2|}\,. \tag{4.9}$$

Here, we retain the function that has an effect on the longest timescales, so the function with the smallest decay rate γ. With this we have,

$$\int_{t_0}^{t}\mathrm{d}t_1\int_{t_0}^{t_1}\mathrm{d}t_2\,|\,\langle \hat{X}(t_1)\hat{X}(t_2)\rangle_0\,| \approx \frac{\lambda}{\gamma}(t-t_0)\,, \tag{4.10}$$

and find an upper bound for the lowest-order correction C_2:

$$\left|\int_{t_0}^{t}\mathrm{d}t_1\int_{t_0}^{t_1}\mathrm{d}t_2\,C_2(t,t_1,t_2)\right| \leq \frac{\lambda}{\gamma}(t-t_0)\left(2|\,\langle \hat{O}(t)\hat{A}(t)\hat{O}(t)\rangle_0\,|\right.$$
$$+|\,\langle \hat{A}(t)\hat{O}(t)\hat{O}(t)\rangle_0\,|$$
$$\left.+|\,\langle \hat{O}(t)\hat{O}(t)\hat{A}(t)\rangle_0\,|\right)\,. \tag{4.11}$$

With this, the self-consistent verification of the condition in Eq. (4.8) can be carried out without the measurement of three-time correlators. Furthermore, only a rough knowledge of the decay behavior of the bath is necessary to find out whether the effect of the bath affects the results of the simulation.

4.5. Short-time and long-time limit

If we assume that the effect of external degrees of freedom in an existing quantum simulator is weak, it is clear that the results are reliable for short times. Unfortunately, it is not clear how long a simulation can take before the reliability is affected. Using our protocol it is possible to determine this timescale. This is illustrated in Sec. 4.6.1 on the basis of a simple toy model. In this section, we examine the time-dependent convergence behavior of the series. With this, we illustrate, that simulations are reliable on a certain timescale and that the expansion usually diverges in the long-time limit. Furthermore, we show that under specific conditions it is even possible that the corrections remain small for all times. An example for this is given in Sec. 4.6.2. Either way, our protocol shows if the simulation is reliable at a certain point in time.

The analysis of the convergence behavior of the series in Eq. (4.5) is carried out under the assumptions that the bath is Markovian and that the bath correlator is described by an exponential decay (see Eq. (4.9)). So we assume that the decay rate γ is the smallest decay rate of the bath but is still large in comparison to the decay rates of the system.

In the following, we describe correlators like $\langle \hat{O}(t_1)\hat{A}(t)\hat{O}(t_2)\rangle_0$ that only contain operators of the system with the term „system correlator". We start with examining the worst-case scenario, where the system correlators do not assist the convergence. We

assume them to be constant in time (c_1). This results in,

$$\int\limits_{t_0}^{t} \mathrm{d}t_1 \int\limits_{t_0}^{t_1} \mathrm{d}t_2 \, \langle \hat{O}(t_1)\hat{A}(t)\hat{O}(t_2)\rangle_0 \, \langle X(t_1)X(t_2)\rangle_0 = c_1\lambda\frac{t-t_0}{\gamma} + c_1\lambda\frac{e^{-\gamma(t-t_0)}-1}{\gamma^2} \,. \quad (4.12)$$

All four terms in Eq. (4.7) show the same behavior with an appropriate constant c_i. We see that they increase with time. This reflects the fact, that the influence of the external degrees of freedom grows with time. But even in this worst-case scenario, there is a timescale where the corrections are small so that the simulation is reliable. In the following, we perform the same analysis for the terms in fourth order. To do this, we assume Wick's theorem to hold for the bath operator $\hat{X}$. This means, that bath correlators can be described as products of two-time correlators (see Eq. (2.13)). Exemplary, we focus on one term of the fourth order,

$$\quad (4.13)$$

The sinusoidal lines correspond to two-time correlators of operator $\hat{X}$. It is known from standard master-equation calculations, that inseparable diagrams, like the last two in this example, decay faster then separable diagrams if the bath correlator decays fast (see Sec. 3.2.1). With this, we can assume that inseparable diagrams can be neglected in comparison to lower orders. Therefore, we focus on the seperable diagram,

$$\text{\raisebox{-0.5em}{[diagram]}} = \int\limits_{t_0}^{t} \mathrm{d}t_1 \int\limits_{t_0}^{t_1} \mathrm{d}t_2 \int\limits_{t_0}^{t_2} \mathrm{d}t_3 \int\limits_{t_0}^{t_3} \mathrm{d}t_4 \langle \hat{X}(t_1)X(t_2)\rangle_0 \langle \hat{X}(t_3)X(t_4)\rangle_0$$

$$\times \, \langle \hat{O}(t_3)\hat{O}(t_1)\hat{A}(t)\hat{O}(t_2)\hat{O}(t_4)\rangle_0 \approx c\lambda^2\frac{(t-t_0)^2}{\gamma^2} \,. \quad (4.14)$$

In the limit $t_0 \to -\infty$, the second order terms grow linear in time. We see here, that the fourth order scales with $(t-t_0)^2$. Higher orders behave accordingly. The corrections diverge for $t_0 \to -\infty$. But on a short timescale, the series converges in this worst-case

scenario.

It is possible that an advantageous behavior of the system correlators extend the time-scale of convergence or even creates convergence of the series for all times. In the latter case, the system correlators have to decay exponentially. With this, the simulator is even reliable on all time scales.

4.6. Model systems

4.6.1. Single qubit with bosonic bath

In this section, we discuss a simple toy model to show that the use of the perturbed system correlators within our self-consistent protocol is able to reveal that the simulation is only reliable for short times. We discuss a very simple model of a single spin,

$$H_S = \frac{1}{2}\epsilon\sigma_z \qquad H_B = \sum_i \epsilon_i b_i^\dagger b_i \qquad H_C = \sigma_x \sum_i f_i(b_i^\dagger + b_i), \qquad (4.15)$$

where bosonic degrees of freedom, described by creation and annihilation operators $b_i^{(\dagger)}$, form the bath. The external degrees of freedom are coupled to the spin via $\hat{O} = \sigma_x$. The full system is the so-called spin-boson model. A single qubit or spin is not an interesting system for an actual quantum simulation, but for this system, it is possible to calculate the perturbed correlators, as needed for the protocol.

When executing our protocol in experiment the perturbed system correlators are measured and used to calculate C_2. In this example, we calculate the perturbed quantities to perform the self-consistent verification in Eq. (4.8).

We assume the bosonic bath to have a flat spectral density. In this case, it is possible to use the approximation in Eq. (4.9) for the correlator of the bath. The effect of the external degrees of freedom is therefore captured in λ and γ. A similar approximation

can also be used for more general situations in the long-time limit. Assuming that the system correlators are approximately constant over a time γ^{-1} we find in the $t_0 \to -\infty$,

$$\int_{t_0}^{t} \mathrm{d}t_1 \int_{t_0}^{t_1} \mathrm{d}t_2 \, C_2(t, t_1, t_2) \approx \frac{2\lambda}{\gamma} \int_{t_0}^{t} \mathrm{d}t_1 \left(\langle \sigma_x(t_1)\hat{A}(t)\sigma_x(t_1) \rangle_0 - \langle \hat{A}(t) \rangle_0 \right) \tag{4.16}$$

since $\sigma_x^2 = \mathbb{1}$. We assume the error to be perturbative so that we can use the perturbed system correlators to calculate C_2,

$$\int_{t_0}^{t} \mathrm{d}t_1 \int_{t_0}^{t_1} \mathrm{d}t_2 \, C_2(t, t_1, t_2) \approx \frac{2\lambda}{\gamma} \int_{t_0}^{t} \mathrm{d}t_1 \left(\langle \sigma_x(t_1)\hat{A}(t)\sigma_x(t_1) \rangle - \langle \hat{A}(t) \rangle \right) \tag{4.17}$$

$$= \frac{2\lambda}{\gamma} \int_{t_0}^{t} \mathrm{d}t_1 \left(\mathrm{Tr}\left[\Pi_{t_1 \to t}(\sigma_x \Pi_{t_0 \to t_1}(\rho_0)\sigma_x)\hat{A} \right] - \mathrm{Tr}\left[\Pi_{t_0 \to t}(\rho_0)\hat{A} \right] \right), \tag{4.18}$$

where $\Pi_{t_1 \to t_2}(\rho)$ represents the time evolution of the spin-boson model. This result is based on the quantum regression theorem. The time evolution of the density matrix of the perturbed system can be found using master-equation calculations in the Born-Markov approximation (see [61]),

$$\Pi_{t_0 \to t}(\rho) = \begin{pmatrix} e^{-\Gamma(t-t_0)}\rho_0^{\uparrow\uparrow} & e^{-\frac{i\epsilon+\Gamma}{2}(t-t_0)}\rho_0^{\uparrow\downarrow} \\ e^{\frac{i\epsilon-\Gamma}{2}(t-t_0)}\rho_0^{\downarrow\uparrow} & 1 - e^{-\Gamma(t-t_0)}\rho_0^{\uparrow\uparrow} \end{pmatrix}, \tag{4.19}$$

where Γ denotes the decay rate of the spin. ρ_0 is the density matrix at time t_0. We assume the system to be prepared in a mixed state,

$$\rho_0 = \begin{pmatrix} a & 0 \\ 0 & 1-a \end{pmatrix}. \tag{4.20}$$

In the limit $t_0 \to -\infty$ we find

$$\Pi^0_{t_1 \to t}(\sigma_x \Pi^0_{t_0 \to t_1}(\rho_0)\sigma_x) - \Pi^0_{t_0 \to t}(\rho_0) = \begin{pmatrix} e^{-\Gamma(t-t_1)} & 0 \\ 0 & -e^{-\Gamma(t-t_1)} \end{pmatrix}. \qquad (4.21)$$

With this, we find the quantity C_2 calculated using the perturbed system correlators

$$\int\limits_{t_0}^{t} \mathrm{d}t_1 \int\limits_{t_0}^{t_1} \mathrm{d}t_2 \, C_2(t, t_1, t_2) \approx \frac{2\lambda}{\gamma\Gamma}(A_{\downarrow\downarrow} - A_{\uparrow\uparrow}). \qquad (4.22)$$

$A_{\uparrow\uparrow}$ and $A_{\downarrow\downarrow}$ describe matrix elements of $\hat{A}$. The transition rate of the spin Γ is induced by the external degrees of freedom whose impact is characterized by λ and γ. Therefore, we have $\Gamma \approx \frac{\lambda}{\gamma}$ and thus the condition in Eq. (4.8) yields in the limit $t_0 \to -\infty$

$$2|A_{\downarrow\downarrow} - A_{\uparrow\uparrow}| \ll |A_{\downarrow\downarrow}|. \qquad (4.23)$$

For example, in the case of $\hat{A} = \sigma_z$ we have shown that our protocol reveals the fact that the simulation is not reliable in the long time limit. This example illustrates that it is advantageous to apply the protocol to different operators $\hat{A}$. This prevents us from certifying reliability accidentally, because $A_{\uparrow\uparrow} \approx A_{\downarrow\downarrow}$. In this example, this happens for $\hat{A}$ in the x-y-plane. It is possible to uncover this mistake with an operator that has a significant contribution from σ_z.

4.6.2. Spin-boson model with additional bosonic bath

In this section, we look at a simulator for the spin-boson model perturbed by additional bosonic degrees of freedom to show, that it is possible that the system correlators create convergence in the long-time limit. Within the Born-Markov approximation (see [61]), we can calculate the system correlators and show that they decay to a stationary value. This decay of the system correlators creates the convergence. Once again, this is a toy

model, since it is possible to solve the system Hamiltonian in this regime. But the setting is similar to proposals [15, 62] of quantum simulators made of qubits and resonators. The model is given by the following Hamiltonians,

$$H_S = \frac{1}{2}\epsilon\sigma_z + \sum_i \omega_i b_i^\dagger b_i + \sigma_x \sum_i t_i(b_i^\dagger + b_i) \tag{4.24}$$

$$H_B = \sum_i \epsilon_i c_i^\dagger c_i \tag{4.25}$$

$$H_C = \sigma_x \sum_i f_i(c_i^\dagger + c_i) \,, \tag{4.26}$$

where $b_i^{(\dagger)}$ and $c_i^{(\dagger)}$ are bosonic creation and annihilation operators. As in the preceding section, we assume a flat spectral density for the bath and use Eq. (4.9) for the bath correlators. The variables characterizing the effect of the external degrees of freedom are λ and γ. Assuming that the system correlators do not vary over time γ^{-1} we can use the results from the preceding section to calculate C_2 in the long-time limit $t_0 \to -\infty$,

$$\int_{t_0}^t dt_1 \int_{t_0}^{t_1} dt_2\, C_2(t, t_1, t_2) \approx \frac{2\lambda}{\gamma} \int_{t_0}^t dt_1 \left(\langle \sigma_x(t_1)\hat{A}(t)\sigma_x(t_1)\rangle_0 - \langle\hat{A}(t)\rangle_0 \right) \tag{4.27}$$

$$= \frac{2\lambda}{\gamma} \int_{t_0}^t dt_1 \left(\mathrm{Tr}\left[\Pi^0_{t_1\to t}(\sigma_x\Pi^0_{t_0\to t_1}(\rho_0)\sigma_x)\hat{A} \right] - \mathrm{Tr}\left[\Pi^0_{t_0\to t}(\rho_0)\hat{A} \right] \right) \,, \tag{4.28}$$

where $\Pi^0_{t_1\to t_2}(\rho)$ is the time evolution of the density matrix of the spin-boson model ($\lambda_B = 0$). It is given by $\Pi_{t_1\to t_2}(\rho)$ from the previous section with $\Gamma = \tilde{\Gamma}$, where $\tilde{\Gamma}$ is the spin decay rate of the spin-boson model without coupling to the external degrees of freedom. With a preparation in a mixed state (Eq. (4.20)) we find in the long-time limit

$$\int_{t_0}^t dt_1 \int_{t_0}^{t_1} dt_2\, C_2(t, t_1, t_2) \propto \frac{\lambda}{\gamma\tilde{\Gamma}} \,. \tag{4.29}$$

We see that the correction C_2 has a finite value in the long-time limit. With this, we have shown that the system correlators can create convergence in the series for all times. At the end of this section, we focus on higher order terms to support this statement. The condition in Eq. (4.8), calculated with the ideal values, reads

$$\frac{2\lambda}{\gamma\tilde{\Gamma}}|A_{\downarrow\downarrow} - A_{\uparrow\uparrow}| \ll |A_{\downarrow\downarrow}|. \tag{4.30}$$

$\tilde{\Gamma}$ is result of bosonic modes of the system. The decay rate $\frac{\lambda}{\gamma}$ is induced by external degrees of freedom. So if the decay rate induced by the external degrees of freedom is small in comparison to the internal decay rate $\tilde{\Gamma}$ the simulator is reliable for all times. This is exactly what is expected. But the protocol is able to reveal if this is this case.

We assumed that a small value of C_2 justifies the assumption that the series converges. Comparing terms of second and fourth order we validate this assumption. We focus on separable diagrams since they cause the main contributions in the limit $t_0 \to -\infty$. The decay of the system correlators, which is necessary for convergence, is assumed to be exponentially $e^{-\kappa(t-t_i)}$. In accordance with the calculations presented above we find in second order

$$\int_{t_0}^{t}\mathrm{d}t_1\int_{t_0}^{t_1}\mathrm{d}t_2\, C_2(t, t_1, t_2) \approx \frac{\lambda}{\gamma\kappa}\left(2\left\langle\hat{O}(t)\hat{A}(t)\hat{O}(t)\right\rangle_0 - \left\langle\hat{O}(t)\hat{O}(t)\hat{A}(t)\right\rangle_0\right.$$
$$\left. - \left\langle\hat{A}(t)\hat{O}(t)\hat{O}(t)\right\rangle_0\right). \tag{4.31}$$

For the fourth order we find accordingly,

$$\int_{t_0}^{t}\mathrm{d}t_1\int_{t_0}^{t_1}\mathrm{d}t_2\int_{t_0}^{t_2}\mathrm{d}t_3\int_{t_0}^{t_3}\mathrm{d}t_4\, C_4(t, t_1, t_2, t_3, t_4) \approx \left(\frac{\lambda}{\gamma\kappa}\right)^2\left(\left\langle\hat{O}(t)\hat{O}(t)\hat{O}(t)\hat{O}(t)\hat{A}(t)\right\rangle_0\right.$$
$$-4\left\langle\hat{O}(t)\hat{O}(t)\hat{O}(t)\hat{A}(t)\hat{O}(t)\right\rangle_0 + 6\left\langle\hat{O}(t)\hat{O}(t)\hat{A}(t)\hat{O}(t)\hat{O}(t)\right\rangle_0$$
$$\left. -4\left\langle\hat{O}(t)\hat{A}(t)\hat{O}(t)\hat{O}(t)\hat{O}(t)\right\rangle_0 + \left\langle\hat{A}(t)\hat{O}(t)\hat{O}(t)\hat{O}(t)\hat{O}(t)\right\rangle_0\right). \tag{4.32}$$

For the case $\hat{O} = \sigma_x$ and $\hat{A} = \sigma_z$, we find

$$\int_{t_0}^t \mathrm{d}t_1 \int_{t_0}^{t_1} \mathrm{d}t_2 \, C_2(t, t_1, t_2) \approx -4\frac{\lambda}{\gamma\kappa} \langle \hat{A}(t) \rangle_0 \tag{4.33}$$

$$\int_{t_0}^t \mathrm{d}t_1 \int_{t_0}^{t_1} \mathrm{d}t_2 \int_{t_0}^{t_2} \mathrm{d}t_3 \int_{t_0}^{t_3} \mathrm{d}t_4 \, C_4(t, t_1, t_2, t_3, t_4) \approx 16\left(\frac{\lambda}{\gamma\kappa}\right)^2 \langle \hat{A}(t) \rangle_0 \, . \tag{4.34}$$

Since the prefactor of the fourth order correction is the prefactor of the second order correction squared, convergence of the series follows from a small value of C_2. In general, this is not true. For example, it is possible that C_2 vanishes for special choices of $\hat{A}$ and $\hat{O}$, whereas C_4 has a finite value. We already proposed to carry out the protocol for several operators $\hat{A}$. Furthermore, it is possible to extend the protocol to higher order corrections to eliminate this situation.

4.7. Generalization

To use the protocol it is important to know, which operator $\hat{O}$ couples the simulator to the dominating source of noise. Applying the protocol with different choices for $\hat{O}$ makes it possible to identify the major perturbation. In the case of coupled qubits, the simulator is not coupled to one bath. Rather, each qubit is coupled individually to independent baths via $H_C = \sum_i \hat{O}_i \hat{X}_i$. The protocol can be directly transferred to this case. We then find sums over system correlators like $\langle \hat{O}_i(t_1) \hat{A}(t) \hat{O}_j(t_2) \rangle_0$. The number of system correlators that have to be measured in the protocol scales with N^2, where N is the number of qubits. Therefore, the effort to carry out the protocol for simulators with a large number of qubits is significant. Analog quantum simulators with qubits coupled to bosonic modes give interesting results using a small number of qubits [62]. For simulators of this kind, our protocol is especially suitable. Since we allow the system Hamiltonian to be time-dependent, the protocol can be applied to digital quantum simulations too. Typically, digital quantum simulations require a large number of qubits. Digital-analog

approaches [15] demand a smaller number of qubits. Applying the protocol to such systems seems particularly reasonable.

Apart from external degrees of freedom, errors in quantum simulations can be a consequence of an imperfect fabrication, which can be described as disorder $H = H_S + \delta H_S$. From standard perturbation theory, we know that the lowest order correction depends on matrix elements of δH_S and stays small at all times. In case of a slowly time-dependent disorder $\delta H_S(t)$, it is expected that ensemble averages have a Gaussian distribution. With this, we arrive at similar results as discussed in this chapter. If the disorder is fluctuating fast the resulting equations are the same as above but with averages of classical random variables instead of the bath correlators. Therefore, the case of disorder can also be covered with a similar self-consistent protocol. Furthermore, the case of gate-errors can also be treated with such a protocol, since it could be described by a term of the form $\delta H_S(t)$.

5. Reconstructing the ideal results of a perturbed analog quantum simulator

Analog quantum simulators are perturbed by external degrees of freedom. In this chapter, we derive an equation that - under certain conditions - connects measurable quantities of a perturbed simulator in thermal equilibrium with the ideal results. This allows for reconstructing the error-free result from a noisy analog quantum simulator. The technique works without adding an overhead to the quantum chip. However, it is only applicable under specific circumstances. The result of the simulation is assumed to be a correlator of the form $\langle \hat{O}^i(t)\hat{O}^j(0)\rangle$, where $\hat{O}^i$ are operators that couple the simulator to the external degrees of freedom. Under the condition that their noise spectral density is known and that the correlators of the bath obey Wick's theorem, it is possible to reconstruct the ideal result. The assumption of Wick's theorem is fundamental for this work, and it is unclear if it is true in the actually considered quantum system. We provide a way to verify this in experiment using additional measurements on the simulator. The work is based on a diagrammatic expansion that includes a resummation of higher order terms. Therefore, this reconstruction method applies potentially also in a regime of intermediate noise strength. Based on an example of a system of coupled resonators we validate the reconstruction equation. This work had been presented before in Ref. [I].

5.1. Introduction

In this chapter, we examine an analog quantum simulator in thermal equilibrium. The measurement result of the simulation is given by a time-ordered correlation function, a so-called Green's function,

$$iG_{S0}(t) = \langle \mathcal{T} \hat{O}(t) \hat{O}(0) \rangle_0 = \langle 0| \, \mathcal{T} \, e^{iH_S t} \hat{O} e^{-iH_S t} \hat{O} \, |0\rangle \, , \qquad (5.1)$$

with time-ordering operator $\mathcal{T}$. We study the system in the zero-temperature limit, where $|0\rangle$ is the ground state of the Hamiltonian H_S that describes the simulator. Green's functions are connected to a lot of interesting quantities, e.g. heat or electric transport coefficients. Several methods to measure the appropriate correlators are proposed in the context of analog quantum simulation [VII, 63–65]. Therefore, we assume that Green's functions are well suited to gain results from a quantum simulation.

The Green's function $G_{S0}(t)$ describes the ideal result of the simulation. External degrees of freedom that are coupled to the simulator will affect the simulation results (see Sec. 2.2). This work is about connecting the perturbed Green's function, that is measured on the real simulator, to the ideal result described by $G_{S0}(t)$. In particular, we are interested in the Green's function of operator $\hat{O}$ which couples the external degrees of freedom to the simulator. With this, the generality of our approach is limited. In principle, it is reasonable to assume, that the operator that couples the system to its external degrees of freedom is also an operator that allows for the readout of the system. In the case of superconducting qubits, two readout mechanisms are common, dispersive readout via σ_z and resonant readout via σ_x. T_1 limited qubits where the readout is performed resonantly and T_2 limited qubits with dispersive readout [66] met our requirement. So the focus on this specific Green's function is justified. Apart from this, the calculations are based on a specific assumption concerning the correlators of operator $\hat{O}$. We require the correlators to obey Wick's theorem so that every n-time correlator can be expressed as sums of products of two-time correlators. This central assumption

is explained in more detail in Sec. 5.1.1. In this work, we derive the connection of the perturbed and the ideal Green's function. To use the result to reconstruct the ideal correlator a knowledge of the spectral density of the bath, that contains the external degrees of freedom, is necessary.

5.1.1. Principal idea

The purpose of this section is to explain our approach using a simplified setting. We consider the full system ($\lambda_B = 1$) consisting of the Hamiltonian H_S describing the simulator, the bath Hamiltonian H_B, and the coupling Hamiltonian H_C (see Sec. 2.1),

$$H = H_S + \lambda_B H_C + H_B \ , \ H_C = \hat{O}\hat{X} \ , \tag{5.2}$$

at zero temperature. Operator $\hat{O}$ couples the system to the external degrees of freedom. The result of the simulation is given by the Green's function of this operator $\hat{O}$. In Sec. 5.4, we extend this model to a more general coupling Hamiltonian and to finite temperatures. The external degrees of freedom are assumed to be bosonic. But it is possible to directly port it to the case of fermionic external degrees of freedom.

The goal is to connect the Green's function of the perturbed simulator $G_{SB}(t)$ to the ideal Green's function $G_{S0}(t)$ and the bath correlator $G_{B0}(t)$. To extract the ideal result from this relation we assume the spectral function of the bath and with this $G_{B0}(t)$ to be known. An overview of all Green's functions is given in Fig. 5.1. A precise definition is given in Sec. 5.4. With standard techniques from many-body physics it is possible to express the full Green's function $G_{SB}(\omega)$ in terms of the ideal Green's functions $G_{S0}(\omega)$ and $G_{B0}(\omega)$ [45]. These techniques require that Wick's theorem applies for the ideal correlators of system and bath (see Sec.2.4). This means, that all ideal correlators of $2n$ operators can be written in terms of n two-time correlators. For system operator $\hat{O}$ it
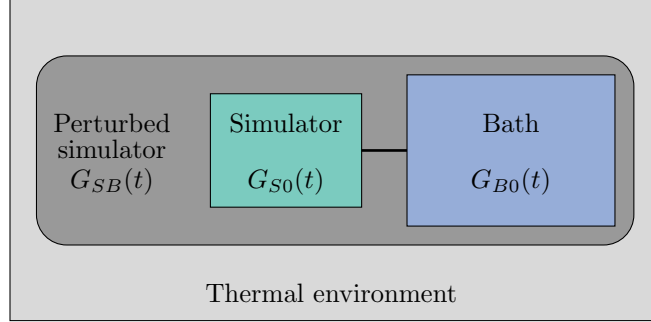
Figure 5.1.: We study a simulator that is perturbed by a bath containing unwanted external degrees of freedom. The whole system is in thermal equilibrium. The different parts of our system are associated with corresponding Green's functions: the ideal Green's function of the simulator $iG_{S0}(t) = \langle \mathcal{T}\hat{O}(t)\hat{O}(0)\rangle_0$ (see Eq. (5.1)) and the free Green's function of the bath $iG_{B0}(t) = \langle \mathcal{T}\hat{X}(t)\hat{X}(0)\rangle_0$. The perturbed simulator is related to the full Green's function $iG_{SB}(t) = \langle \mathcal{T}\hat{O}(t)\hat{O}(0)\rangle$. Reprinted with permission of Ref. [I]. Copyright (2018) by the American Physical Society.

reads,

$$
\begin{aligned}
&\langle \mathcal{T}\hat{O}(t_1)\hat{O}(t_2)\ldots\hat{O}(t_{n-1})\hat{O}(t_n)\rangle_0 \\
&= \langle \mathcal{T}\hat{O}(t_1)\hat{O}(t_2)\rangle_0 \langle \mathcal{T}\hat{O}(t_3)\ldots\hat{O}(t_{n-1})\hat{O}(t_n)\rangle_0 \\
&+ \langle \mathcal{T}\hat{O}(t_1)\hat{O}(t_3)\rangle_0 \langle \mathcal{T}\hat{O}(t_2)\ldots\hat{O}(t_{n-1})\hat{O}(t_n)\rangle_0 \\
&+ \ldots + \langle \mathcal{T}\hat{O}(t_1)\hat{O}(t_n)\rangle_0 \langle \mathcal{T}\hat{O}(t_2)\ldots\hat{O}(t_{n-1})\rangle_0 \,.
\end{aligned}
\tag{5.3}
$$

Especially, we assume that operators $\hat{O}(t)$ follow a bosonic Wick's theorem, where no sign changes occure for permutations of $\hat{O}(t)$. Applying this iteratively it is possible to represent an n-time correlator only with two-time correlators. The assumption that Wick's theorem holds for the bath operator $\hat{X}$ complies with standard system-bath approaches. Whereas, for correlators of the system operator $\hat{O}$ Wick's theorem cannot be assumed to be true in general. For a situation where the system Hamiltonian can be described using non-interacting quasiparticles and $\hat{O}$ is given by a linear combination of the annihilation and creation operators of these quasiparticles, it is known that Wick's

theorem holds. Generally, Wick's theorem is valid in situations where fluctuations of $\hat{O}(t)$ have a Gaussian distribution. Deviations from Gaussian statistics have been examined in the field of full-counting statistics [32, 67–69]. The central limit theorem [70] is the basis for the anticipation that fluctuations become more Gaussian with increasing system size. This is also the most interesting limit for a quantum simulator. But systems exist where non-Gaussian fluctuations are known to persist even at large system size [71, 72] or become even size independent [73]. A mapping of qubits coupled to bosonic baths to an effective electron-phonon model [II] could be of interest in some expansions. Due to the fact that the assumption of Wick's theorem is crucial for our theory, we present a possibility to validate this assumption with additional measurements on the perturbed quantum simulator (see Sec. 5.2).

Based on the standard many-body methods and the assumption of Wick's theorem we find the well-known Dyson equation,

$$G_{SB}(\omega) = G_{S0}(\omega) + G_{S0}(\omega) G_{B0}(\omega) G_{SB}(\omega)\,, \tag{5.4}$$

connecting the full Green's function with the free Green's functions of system and bath.

5.1.2. Central result

With Eq. (5.4) we can express the ideal Green's function of the system in terms of the Green's function of the perturbed system and the bath

$$G_{S0}(\omega) = \frac{G_{SB}(\omega)}{1 + G_{B0}(\omega) G_{SB}(\omega)}\,. \tag{5.5}$$

With an appropriate knowledge of the bath correlator $G_{B0}(\omega)$ it is possible to calculate the ideal result based on measurements on the perturbed simulator. This equation is the central result of this work in a very simple form. It is based on the assumption that Wick's theorem holds for correlators of the system operator $\hat{O}$. In Sec. 5.2 we discuss

this assumption in more detail and how to validate this in lowest order. Furthermore, the quality of the reconstruction depends on the knowledge of the correlators. This is discussed in Sec. 5.3. The properties of the bath are assumed to be characterized independently of the system (see Sec. 2.3). An extension to more realistic coupling Hamiltonians and to finite temperatures is subject of Sec. 5.4. Furthermore, even a generalization to time-dependent systems is conceivable using the Keldsyh formalism. This would allow for reconstructing results in non-equilibrium analog quantum simulators and in digital quantum simulators. But this is not shown in this work. Finally, in Sec. 5.4.4 we look at a simple example and solve it analytically to validate the reconstruction equation.

5.2. Verifying Wick's theorem

The assumption of Wick's theorem for operator $\hat{O}$ is substantial for the derivation of Eq. (5.5). For non-trivial systems, as they are of interest for quantum simulations, it is not possible to tell whether this is true. In this section, we give a method to validate the assumption of Wick's theorem in experiment. The detailed derivation is presented in Appendix B.

As basis for this, we define the lowest order correction to Wick's theorem $G_4(t_1, t_2, t_3, t_4)$,

$$
\begin{aligned}
G_4(t_1, t_2, t_3, t_4) &= \langle \mathcal{T} \hat{O}_1 \hat{O}_2 \hat{O}_3 \hat{O}_4 \rangle_{0,F} - \langle \mathcal{T} \hat{O}_1 \hat{O}_2 \hat{O}_3 \hat{O}_4 \rangle_0 \qquad (5.6)\\
&= \langle \mathcal{T} \hat{O}_1 \hat{O}_2 \hat{O}_3 \hat{O}_4 \rangle_{0,F} - \sum_{\substack{3 \text{ perm.} \\ a,b,c,d \\ \in \{1,2,3,4\}}} \langle \mathcal{T} \hat{O}_a \hat{O}_b \rangle_0 \langle \mathcal{T} \hat{O}_c \hat{O}_d \rangle_0 \ ,
\end{aligned}
$$

where we introduce the abbreviation $\hat{O}_i = \hat{O}(t_i)$. For the purpose of this work, we consider corrections in first order of G_4. Index F indicates correlators that include corrections to Wick's theorem. This means $\langle \ldots \rangle_0$ and $\langle \ldots \rangle$ are correlators where Wick's theorem is exactly valid. Whereby, index 0 refers to correlators without coupling to external degrees of freedom. In the second term, Wick's theorem is applied for the

four-time correlator. Therefore, we sum over all indistinguishable permutations. $\langle\ldots\rangle_F$ ($\langle\ldots\rangle_{0,F}$) are (un)perturbed correlators with corrections to Wick's theorem. Correlators measured on the simulator in experiment are of type $\langle\ldots\rangle_F$. A measurement of two- and four-time correlators,

$$\langle\mathcal{T}\hat{O}_1\hat{O}_2\hat{O}_3\hat{O}_4\rangle_F - \sum_{\substack{3\text{ perm.} \\ a,b,c,d \\ \in\{1,2,3,4\}}} \langle\mathcal{T}\hat{O}_a\hat{O}_b\rangle_F\langle\mathcal{T}\hat{O}_c\hat{O}_d\rangle_F = \text{\Large\textbf{X}}\,, \tag{5.7}$$

yields the following quantity

$$\tag{5.8}$$

The thin cross depicts G_4, straight lines depict G_{S0}, and the bath Green's function is represented by sinuous lines. Important is, that this quantity describes the deviation of the perturbed correlator from Wick's theorem,

$$\langle\mathcal{T}\hat{O}_1\hat{O}_2\rangle_F = \langle\mathcal{T}\hat{O}_1\hat{O}_2\rangle + \text{\Large\textbf{X}}\,. \tag{5.9}$$

In combination with the knowledge of the bath Green's function, a measurement of two- and four-time correlators of $\hat{O}$ allows to check whether Wick's theorem is valid. With this, we find out if the reconstruction of the ideal Green's function is possible.

5.3. Imperfect knowledge

To use Eq. (5.5) to reconstruct the ideal result, knowledge of the perturbed Green's function G_{SB} and of the bath correator G_{B0} is necessary. However, in reality these quantities are not available in full accuracy. How an imperfect knowledge of these input variables influence the result of the reconstruction is subject of this section.

5.3.1. Bath correlator

Adding a variation to the Green's function of the bath $G_{B0}(\omega) + \delta G_{B0}(\omega)$ transforms Eq. (5.5) to

$$\tilde{G}_{S0}(\omega) = \frac{G_{SB}(\omega)}{1 + G_{B0}(\omega)G_{SB}(\omega) + \delta G_{B0}(\omega)G_{SB}(\omega)} \, . \tag{5.10}$$

With $|\delta G_{B0}(\omega)| \ll |G_{SB}^{-1}(\omega) + G_{B0}(\omega)|$, we find

$$\tilde{G}_{S0}(\omega) \approx G_{S0}(\omega)[1 - G_{S0}(\omega)\delta G_{B0}(\omega)] \, . \tag{5.11}$$

We see, that the influence of $\delta G_{B0}(\omega)$ is large at the peaks of $G_{S0}(\omega)$. The quality of the reconstruction depends on the absolute error $\delta G_{B0}(\omega)$.

5.3.2. Full system correlator

A deviation of the perturbed Green's function $G_{SB}(\omega) + \delta G_{SB}(\omega)$ results in,

$$\tilde{G}_{S0}(\omega) = \frac{G_{SB}(\omega) + \delta G_{SB}(\omega)}{1 + G_{B0}(\omega)G_{SB}(\omega) + G_{B0}(\omega)\delta G_{SB}(\omega)} \, . \tag{5.12}$$

With $|\delta G_{SB}(\omega)| \ll |G_{B0}^{-1}(\omega) + G_{SB}(\omega)|$, we find

$$\tilde{G}_{S0}(\omega) \approx G_{S0}(\omega) \left(1 + \frac{G_{S0}(\omega)}{G_{SB}(\omega)} \frac{\delta G_{SB}(\omega)}{G_{SB}(\omega)} \right) \, . \tag{5.13}$$

Due to the prefactor $G_{S0}(\omega)/G_{SB}(\omega)$ the impact of the variation is large at the peaks of this function. Here, the relative error $\delta G_{SB}(\omega)/G_{SB}(\omega)$ is relevant.

Furthermore, we learn from this equation the fundamental limit of the reconstruction method. Eq. (5.5) is valid for large coupling strength, since it incorporates a resummation of all orders. However, a reconstruction is not possible in this limit if the peaks

of $G_{S0}(\omega)$ are significantly widened, so that $G_{S0}(\omega)/G_{SB}(\omega) \gg 1$ at the peaks. In this case, even a small relative error in $G_{SB}(\omega)$ excludes the possibility of a reliable reconstruction.

5.4. Full model and discussion

The purpose of this section is to consider a more realistic and more general coupling Hamiltonian and to explain the derivation of the generalized version of Eq. (5.5). As described in Sec. 2.1, we consider a system coupled to multiple independent baths,

$$H = H_S + \lambda_B H_C + \sum_{i=1}^{N} H_B^i \qquad H_C = \sum_{i=1}^{N} \hat{O}^i \hat{X}^i \,, \tag{5.14}$$

with $[H_B^i, H_B^j] = 0$.

5.4.1. The full Green's function

The Green's function of operators $\hat{O}^i$ measured on the full system, including the coupling to external degrees of freedom, is $\mathbf{G}_{SB}$ with

$$G_{SB}^{ij}(t) = -i \langle \mathcal{T} \hat{O}^i(t) \hat{O}^j(0) \rangle \,, \tag{5.15}$$

where $\langle \ldots \rangle$ indicates an expectation value of the ground state of the full Hamiltonian. The time evolution operator is given by

$$U_{\lambda_B}(t) = e^{-iHt} \,, \tag{5.16}$$

and transformations to appropriate pictures follow from

$$\hat{A}(t) = U_{\lambda_B}^{-1}(t)\, \hat{A}\, U_{\lambda_B}(t)\,. \tag{5.17}$$

In perturbed correlators $\langle\ldots\rangle$ the full time evolution with $\lambda_B = 1$ is used, which corresponds to the Heisenberg picture. However, in unperturbed correlators $\langle\ldots\rangle_0$, the operators are in interaction picture since $\lambda_B = 0$ applies. With the time evolution operator in interaction picture (see Eq. (2.9)) for infinite times

$$\mathcal{U}(\infty) = \mathcal{T} e^{-i\int_{-\infty}^{\infty} \mathrm{d}t\, H_{C,I}(t)}\,, \tag{5.18}$$

the full Green's function can be expressed by (see Sec. 2.4)

$$G_{SB}^{ij}(t) = -i\frac{\langle\mathcal{T}\mathcal{U}(\infty)\hat{O}^i(t)\hat{O}^j(0)\rangle_0}{\langle\mathcal{T}\mathcal{U}(\infty)\rangle_0}\,. \tag{5.19}$$

The Fourier transform of a Green's function is defined as

$$G_X^{ij}(\omega) = \int_{-\infty}^{\infty} \mathrm{d}t\, e^{i\omega t}\, G_X^{ij}(t)\,. \tag{5.20}$$

5.4.2. Diagrammatic expansion

Assuming Wick's theorem holds for $\hat{O}^i$, we show in this section the diagrammatic expansion that yields the reconstruction equation similar to Eq. (5.5). We use an expansion of $\mathcal{U}(\infty)$ in H_C in Eq. (5.19). With this, the Green's function of the perturbed system can be expressed in terms of the unperturbed Green's functions:

$$\begin{aligned}
&= \;\text{—}\; + \;\text{—o̴wo—}\; + \;\text{—o̴wo—o̴wo—}\; + \ldots \\
&= \;\text{—}\; + \;\text{—o̴wo}(\text{—} + \text{—o̴wo—}\ldots) \\
&= \;\text{—}\; + \;\text{—o̴wo}= \,. \tag{5.21}
\end{aligned}$$

Green's function	Matrix form	Diagram	Definition
$G_{SB}^{ij}(t) = -i\langle \mathcal{T}\hat{O}^i(t)\hat{O}^j(0)\rangle$	$[\mathbf{G}_{SB}]_{ij} = G_{SB}^{ij}$	═══	full Green's function of system operators, including the effects of the bath $(\lambda_B = 1)$
$G_{S0}^{ij}(t) = -i\langle \mathcal{T}\hat{O}^i(t)\hat{O}^j(0)\rangle_0$	$[\mathbf{G}_{S0}]_{ij} = G_{S0}^{ij}$	———	free Green's function of system operators, without the effects of the bath $(\lambda_B = 0)$
$G_{B0}^{ij}(t) = -i\langle \mathcal{T}\hat{X}^i(t)\hat{X}^j(0)\rangle_0$	$[\mathbf{G}_{B0}]_{ij} = G_{B0}^{ij}$	∿∿∿	free Green's function of the bath, without the effects of the system $(\lambda_B = 0)$

Table 5.1.: Summary of all relevant correlators and their diagrammatic representations.

Table 5.1 shows the diagrammatic representations of all Green's functions. The interaction term is displayed in Table 5.2.

The disconnected diagrams are canceled by the vacuum diagrams $\langle \mathcal{T}\mathcal{U}(\infty)\rangle_0$ (see Sec. 2.4). This is shown explicitly in Appendix A. The diagrammatic expansion directly leads to the Dyson equation

$$\mathbf{G}_{SB}(\omega) = \mathbf{G}_{S0}(\omega) + \mathbf{G}_{S0}(\omega)\mathbf{G}_{B0}(\omega)\mathbf{G}_{SB}(\omega). \tag{5.22}$$

The self energy of this Dyson equation is the Green's function of the bath. Thereby, the self energy consists of only one term and there is no need to truncate the series for the self energy as in Chap. 3. Based on the knowledge of the Green's function $G_{SB}^{ij}(\omega)$ and

Interaction	Diagram	Definition
$\sum_{i=1}^{N} \hat{O}^i \hat{X}^i$	—o∿∿	Interaction between bath and system.
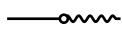
Table 5.2.: Each circle represents a term of the expansion in H_C.

$G_{B0}^{ij}(\omega)$ the Dyson equation can be solved for the ideal Green's function of the simulator $\mathbf{G}_{S0}$:

$$\mathbf{G}_{S0}(\omega) = \mathbf{G}_{SB}(\omega) \left[1 + \mathbf{G}_{B0}(\omega)\mathbf{G}_{SB}(\omega) \right]^{-1} . \tag{5.23}$$

Focusing on a situation with coupling to a single bath reduces this result to the one presented in the beginning (Eq. 5.5).

5.4.3. Extension to finite temperatures

Using the Matsubara formalism we can generalize the diagrammatic expansion, and with this the reconstruction equation Eq. (5.23), to situations with finite temperature. In this section, we introduce the Matsubara Green's functions $\mathcal{G}_{M,X}$ in imaginary time and show how they are connected to the retarded real-time Green's functions $\mathcal{G}_X^R$ for finite temperatures. By analogy, we find for the case of the simple coupling Hamiltonian with one bath

$$\mathcal{G}_{S0}^R(i\omega_n) = \frac{\mathcal{G}_{SB}^R(i\omega_n)}{1 + \mathcal{G}_{B0}^R(i\omega_n)\mathcal{G}_{SB}^R(i\omega_n)} . \tag{5.24}$$

Expansion in imaginary time

The standard Matsubara Green's function method allows us to study systems in thermal equilibrium (see Sec. 2.4). For this, we introduce the imaginary time $\tau = it$ with $0 < \tau < \beta$. The equivalent to Eq. (5.15) in Matsubara formalism reads

$$\mathcal{G}_{M,SB}^{ij}(\tau) = -\langle \mathcal{T}\hat{O}^i(\tau)\hat{O}^j(0)\rangle , \tag{5.25}$$

with $\mathcal{T}$ being the time-ordering operator for imaginary times τ and $\langle \ldots \rangle$ representing the equilibrium expectation value $\mathrm{Tr}(\frac{1}{Z}e^{-\beta H} \ldots)$ with $Z = \mathrm{Tr}(e^{-\beta H})$. In this context,

$\langle\ldots\rangle_0$ indicates the equilibrium expectation value of the ideal system with $\lambda_B = 0$. With the time evolution operator in imaginary time

$$S_{\lambda_B}(\tau) = e^{-H\tau}, \tag{5.26}$$

the transformation of operator $\hat{A}$ in appropriate pictures follows from

$$\hat{A}(\tau) = S_{\lambda_B}^{-1}(\tau)\, \hat{A}\, S_{\lambda_B}(\tau). \tag{5.27}$$

In $\langle\ldots\rangle_0$ the transformation with $S_{\lambda_B=0}$ is implied, $S_{\lambda_B=1}$ is used in $\langle\ldots\rangle$. The perturbed Green's function is given by

$$\mathcal{G}_{M,SB}(\tau) = -\frac{\langle\mathcal{T}\mathcal{S}(\beta)\hat{O}^i(\tau)\hat{O}^j(0)\rangle_0}{\langle\mathcal{T}\mathcal{S}(\beta)\rangle_0}, \tag{5.28}$$

with the time evolution operator in interaction picture

$$\mathcal{S}(\tau) = \mathcal{T}e^{-\int_0^\tau d\tau' H_{C,I}(\tau')}. \tag{5.29}$$

In analogy to the zero temperature case, the disconnected diagrams are canceled by the vacuum diagrams $\langle\mathcal{T}\mathcal{S}(\beta)\rangle_0$. Due to the periodicity in τ with period β Matsubara Green's functions are transformed into frequency space with the discrete Fourier transform with the Matsubara frequencies $\omega_n = 2\pi n/\beta$,

$$\mathcal{G}_{M,X}^{ij}(\tau) = \frac{1}{\beta}\sum_n \mathcal{G}_{M,X}^{ij}(\omega_n)e^{-i\omega_n\tau} \tag{5.30}$$

Connecting a real time correlator to the Matsubara Green's function

The Matsubara Green's functions are objects in imaginary time. In this section, we show the connection to real-time quantities that are measurable. We discuss this with the example of the bath Green's function.

The retarded Green's function of the bath is defined as

$$\mathcal{G}_{B0}^{R,ii}(t) = -i \langle [\hat{X}^i(t), \hat{X}^i(0)] \rangle_0 \, \theta(t) \,. \tag{5.31}$$

The imaginary part of this Green's function is given by the correlator

$$C^i(t) = \left(\langle \hat{X}^i(t)\hat{X}^i(0) \rangle_0 - \langle \hat{X}^i(0)\hat{X}^i(t) \rangle_0 \right) \theta(t) \,, \tag{5.32}$$

except from a factor -1. Defining the eigenstates and eigenenergies of the bath Hamiltonian as $H_B|n\rangle = E_n|n\rangle$, the correlator is given by

$$C^i(t) = \frac{\theta(t)}{Z_B} \sum_{nm} |\langle n|\hat{X}^i|m\rangle|^2 e^{i(E_n - E_m)t} \left(e^{-\beta E_n} - e^{-\beta E_m} \right), \tag{5.33}$$

where $Z_B = \mathrm{Tr}(e^{-\beta H_B})$ is the partition function. The real part of the correlator in frequency space is the spectral function $A^i(\omega)$

$$A^i(\omega) = \frac{1}{\pi} \mathrm{Re} \left(\int_{-\infty}^{\infty} \mathrm{d}t \, e^{i\omega t} C^i(t) \right) \tag{5.34}$$

$$= \frac{1}{Z_B} \sum_{nm} |\langle n|\hat{X}^i|m\rangle|^2 (e^{-\beta E_m} - e^{-\beta E_n}) \, \delta[\omega - (E_n - E_m)] \,. \tag{5.35}$$

If the spectral function was measured, it is possible to calculate the retarded Green's function with

$$\mathcal{G}_{B0}^{R,ii}(\omega) = \int_{-\infty}^{\infty} \mathrm{d}\omega_1 \frac{A^i(\omega_1)}{\omega - \omega_1 + i0} \,. \tag{5.36}$$

Writing the Matsubara Green's function using the spectral function

$$\mathcal{G}_{M,B0}^{ii}(\omega_n) = \int_{-\infty}^{\infty} \mathrm{d}\omega_1 \frac{A^i(\omega_1)}{i\omega_n - \omega_1} \,, \tag{5.37}$$

gives us the connection to the retarded Green's function

$$\mathcal{G}^{ij}_{M,P}(\omega_n) = \mathcal{G}^{R,ij}_P(i\omega_n) \,, \; \omega_n > 0 \,, \tag{5.38}$$

with $P \in \{B0, S0, SB\}$, which involves an analytical continuation of the retarded Green's function in the complex plain. The expression of the Green's functions in terms of the spectral function also leads to the well-known Kramers-Kronig relation

$$\mathcal{G}^{ij}_P(\omega) = \mathrm{Re}\mathcal{G}^{R,ij}_P(\omega) + i(1 + 2\bar{n}(\omega))\mathrm{Im}\mathcal{G}^{R,ij}_P(\omega) \,, \tag{5.39}$$

with $\bar{n}(\omega) = (e^{\beta\omega} - 1)^{-1}$.

Measuring the spectral functions of bath and perturbed system allows us to calculate the respective Matsubara Green's function (see Eq. (5.37)). The reconstruction equation yields the Matsubara Green's function of the ideal system $G^{ij}_{M,S0}(\omega_n)$ and with this the retarded Green's function at the points $i\omega_n$ (see Eq. (5.24)). However, we want to obtain the ideal Green's function $\mathcal{G}^R_{S0}$ or the respective spectral function on the complete real axis. This is possible with numerical methods like the Padé approximation [74]. Nevertheless, the extension of a Green's function from the Matsubara points to the real axis is still an active research field [75].

5.4.4. Model system: chain of resonators with individual baths

In this section, we validate our main result, Eq. (5.22), with a model system. For this purpose, we have to choose a simple model system, where it is possible to calculate the perturbed Green's functions, for example, using master equation approaches. We concentrate on a system of N coupled harmonic oscillators with periodic boundary con-

ditions in thermal equilibrium

$$H_S = \sum_{j=1}^{N} \left(\frac{1}{2} m \omega_r^2 q_j^2 + \frac{1}{2m} p_j^2 + \frac{m\Omega^2}{2} (q_{j+1} - q_j)^2 \right) . \tag{5.40}$$

The uncoupled oscillators are characterized by mass m and eigenfrequency ω_r, Ω denotes the coupling strength of neighboring oscillators. Since Wick's theorem is valid for this system it is suitable to validate the reconstruction equation. However, this system is by construction, not an interesting quantum simulator. For interesting simulators, a calculation of the Green's functions of the system and moreover Green's functions of the perturbed system is not possible. Proposals exist for analog quantum simulators consisting of coupled oscillators, for example for a simulation of the Bose-Hubbard model [76, 77].

The perturbation arises from a coupling of each oscillator to bosonic degrees of freedom

$$H_C = \sum_{j} \hat{O}^j \hat{X}^j , \quad H_B = \sum_{j,m} \bar{\omega}_m^{(j)} b_m^{(j)\dagger} b_m^{(j)} , \tag{5.41}$$

$$\text{with } \hat{O}^j = q_j , \text{ and } \hat{X}^j = \sum_{m} t_m^{(j)} (b_m^{(j)\dagger} + b_m^{(j)}) .$$

The baths are identical

$$\bar{\omega}_m^{(j)} = \bar{\omega}_m , \quad t_m^{(j)} = t_m , \tag{5.42}$$

but independent

$$\langle \hat{X}^{j_1}(t_1) \hat{X}^{j_2}(t_2) \rangle_0 = 0 \text{ for } j_1 \neq j_2 . \tag{5.43}$$

The system Hamiltonian is diagonal in the creation and annihilation operators a_k and

$a_k^\dagger$

$$H_S = \sum_k \Omega_k a_k^\dagger a_k\,, \ \text{ with } \Omega_k = \sqrt{\left[2\Omega \sin(k\frac{\varphi_0}{2})\right]^2 + \omega_r^2}\,, \tag{5.44}$$

with $\varphi_0 = \frac{2\pi}{N}$. They are connected to the original operators in the following way

$$q_j = \sqrt{\frac{1}{2m\omega_r}}(d_j^\dagger + d_j)\,, \tag{5.45}$$

$$d_j = \frac{1}{2\sqrt{N}} \sum_{k=1}^N \left[e^{-ikj\varphi_0} \left(\sqrt{\frac{\omega_r}{\Omega_K}} - \sqrt{\frac{\Omega_K}{\omega_r}} \right) a_k^\dagger + e^{ijk\varphi_0} \left(\sqrt{\frac{\omega_r}{\Omega_K}} + \sqrt{\frac{\Omega_K}{\omega_r}} \right) a_k \right]. \tag{5.46}$$

To validate the reconstruction equation it is necessary to calculate the perturbed Green's function of the system $\mathcal{G}_{M,SB}^{j_1 j_2}$. This is achieved using a standard master equation approach and the quantum regression theorem (QRT) [29]. We approximately describe the perturbed system by a Lindblad equation

$$\dot\rho(t) = \mathcal{L}\rho(t)\,, \tag{5.47}$$

where the Lindblad terms are

$$\mathcal{L}\rho = -i[H_S, \rho] + \sum_{k=1}^N \frac{\Gamma_k}{2}(\bar n_k + 1)\left(2a_k\rho a_k^\dagger - a_k^\dagger a_k\rho - \rho a_k^\dagger a_k\right)$$

$$+ \sum_{k=1}^N \frac{\Gamma_k}{2}\bar n_k \left(2a_k^\dagger \rho a_k - a_k a_k^\dagger \rho - \rho a_k a_k^\dagger\right)\,, \tag{5.48}$$

and $\bar n_k = (e^{\beta\Omega_k} - 1)^{-1}$. Since we assume finite temperatures the spectral density of the bath is given by

$$A^i(\omega) \approx \frac{1}{2\pi}\text{sign}(\omega)J^i(|\omega|)\,, \tag{5.49}$$

with $J^i(\omega) = J(\omega) = 2\pi \sum_m t_m^2 \delta(\omega - \bar{\omega}_m)$. Assuming a smooth spectral density the effective rates are

$$\Gamma_k = \frac{1}{2m\Omega_k} J(\Omega_k) \,. \tag{5.50}$$

The prefactor is explained by the connection of $\hat{O}^i$ to $a_k^{(\dagger)}$. A factor $(2m\omega_r)^{-1}$ is a result from $\hat{O}^i = \sqrt{2m\omega_r}^{-1}(d_j^\dagger + d_j)$ and $\frac{\omega_r}{\Omega_k}$ arises from the transition from $d_j^\dagger + d_j$ to $a_k^\dagger + a_k$.

Calculating the retarded bath Green's function form Eq. (5.36) using the same assumptions as for the Lindblad equation we find

$$i\mathcal{G}_{B0}^{R,ij}(\omega) \approx \delta_{ij}\frac{1}{2}\text{sign}(\omega)J^i(|\omega|) \,. \tag{5.51}$$

Now we calculate the perturbed and free Green's functions of the system and use Eq. (5.22) to obtain the bath Green's function. If the result is in accordance with the above equation we have validated the reconstruction equation.

Due to the QRT the following equation is fulfilled for the Lindblad terms and an arbitrary operator $\hat{A}$ and all k [29]:

$$\text{Tr}\left[a_k\mathcal{L}\hat{A}\right] = -(i\Omega_k + \frac{\Gamma_k}{2})\text{Tr}\left[a_k\hat{A}\right] \,. \tag{5.52}$$

With this we find for $t > 0$

$$\langle\hat{A}(t_0)a_k(t + t_0)\rangle = e^{-i\Omega_k t}e^{-\frac{\Gamma_k}{2}t}\langle\hat{A}(t_0)a_k(t_0)\rangle \,, \tag{5.53}$$

$$\langle a_k(t + t_0)\hat{A}(t_0)\rangle = e^{-i\Omega_k t}e^{-\frac{\Gamma_k}{2}t}\langle a_k(t_0)\hat{A}(t_0)\rangle \,, \tag{5.54}$$

$$\langle\hat{A}(t_0)a_k^\dagger(t + t_0)\rangle = e^{+i\Omega_k t}e^{-\frac{\Gamma_k}{2}t}\langle\hat{A}(t_0)a_k^\dagger(t_0)\rangle \,, \tag{5.55}$$

$$\langle a_k^\dagger(t + t_0)\hat{A}(t_0)\rangle = e^{+i\Omega_k t}e^{-\frac{\Gamma_k}{2}t}\langle a_k^\dagger(t_0)\hat{A}(t_0)\rangle \,. \tag{5.56}$$

Correlators of the form $\langle a_k^{(\dagger)}(t_0)a_k^{(\dagger)}(t_0)\rangle$ can be calculated using the information that the stationary solution of the Lindblad equation is proportional to $e^{-\beta\sum_k \Omega_k a_k^\dagger a_k}$. With this

we find the results for the perturbed correlators

$$\langle a_k(t_1) a_{k'}(t_2) \rangle = 0 \,, \tag{5.57}$$

$$\langle a_k^\dagger(t_1) a_{k'}(t_2) \rangle = \delta_{k,k'} \bar{n}_k e^{i\Omega_k(t_1-t_2)} e^{-\frac{\Gamma_k}{2}|t_1-t_2|} \,, \tag{5.58}$$

$$\langle a_k(t_1) a_{k'}^\dagger(t_2) \rangle = \delta_{k,k'} (\bar{n}_k + 1) e^{i\Omega_k(t_1-t_2)} e^{-\frac{\Gamma_k}{2}|t_1-t_2|} \,, \tag{5.59}$$

$$\langle a_k^\dagger(t_1) a_{k'}^\dagger(t_2) \rangle = 0 \,. \tag{5.60}$$

Based on this, we will calculate the perturbed Green's function in the next step. But previously we present the results for the according free correlators that we need for calculating the unperturbed Green's function

$$\langle a_k(t_1) a_{k'}(t_2) \rangle_0 = 0 \,, \tag{5.61}$$

$$\langle a_k^\dagger(t_1) a_{k'}(t_2) \rangle_0 = \delta_{k,k'} \bar{n}_k e^{i\Omega_k(t_1-t_2)} \,, \tag{5.62}$$

$$\langle a_k(t_1) a_{k'}^\dagger(t_2) \rangle_0 = \delta_{k,k'} (\bar{n}_k + 1) e^{i\Omega_k(t_1-t_2)} \,, \tag{5.63}$$

$$\langle a_k^\dagger(t_1) a_{k'}^\dagger(t_2) \rangle_0 = 0 \,. \tag{5.64}$$

With the knowledge of these correlators it is possible to calculate the retarded perturbed and unperturbed Green's functions of the system $\mathcal{G}_{S0}^{R,j_1 j_2}(t)$, $\mathcal{G}_{SB}^{R,j_1 j_2}(t)$. Using a Fourier transform and an analytical continuation we obtain the Matsubara Green's functions for $\omega_n > 0$ (see Eq. (5.38)):

$$\mathcal{G}_{M,SO}^{j_1 j_2}(\omega_n) = \frac{1}{N} \sum_{k=1}^N \frac{1}{2m\Omega_k} \times \left[e^{-ik(j_1-j_2)\varphi_0} \bar{n}_k - e^{ik(j_1-j_2)\varphi_0} (\bar{n}_k + 1) \right]$$
$$\times \left(\frac{1}{i\omega_n + \Omega_k + i0} - \frac{1}{i\omega_n - \Omega_k + i0} \right) \,, \tag{5.65}$$

$$\mathcal{G}_{M,SB}^{j_1 j_2}(\omega_n) = \frac{1}{N} \sum_{k=1}^N \frac{1}{2m\Omega_k} \times \left[e^{-ik(j_1-j_2)\varphi_0} \bar{n}_k - e^{ik(j_1-j_2)\varphi_0} (\bar{n}_k + 1) \right]$$
$$\times \left(\frac{1}{i\omega_n + \Omega_k + i\frac{\Gamma_k}{2}} - \frac{1}{i\omega_n - \Omega_k + i\frac{\Gamma_k}{2}} \right) \,. \tag{5.66}$$

We valdiate the Matsubara equivalent of the reconstruction equation Eq. (5.22) by calculating the bath Green's function using this equation and compare it to Eq. (5.51). To do this, we introduce the following transformation

$$\mathcal{G}^k_{M,S0}(\omega_n) = \sum_{j_1,j_2} \mathcal{G}^{j_1 j_2}_{M,SO} e^{ik(j_1-j_2)k\varphi_0}$$
$$= \frac{N}{2m\Omega_k} \left(\frac{1}{i\omega_n - \Omega_k + i0} - \frac{1}{i\omega_n + \Omega_k + i0} \right), \tag{5.67}$$

$$\mathcal{G}^k_{M,SB}(\omega_n) = \sum_{j_1,j_2} \mathcal{G}^{j_1 j_2}_{M,SB} e^{ik(j_1-j_2)k\varphi_0}$$
$$= \frac{N}{2m\Omega_k} \left(\frac{1}{i\omega_n - \Omega_k + i\frac{\Gamma_k}{2}} - \frac{1}{i\omega_n + \Omega_k + i\frac{\Gamma_k}{2}} \right). \tag{5.68}$$

and find for Eq. (5.23)

$$\mathcal{G}^k_{M,SB}(\omega_n) = \mathcal{G}^k_{M,S0}(\omega_n) + \mathcal{G}^k_{M,S0}(\omega_n)\mathcal{G}^k_{M,SB}(\omega_n) \times \sum_j \mathcal{G}^{jj}_{M,BO}(\omega_n) \frac{1}{N^2}. \tag{5.69}$$

With this, we calculate the Green's function of the bath

$$\mathcal{G}^{j_1 j_2}_{M,BO}(\omega_n \approx \Omega_k) \approx \delta_{j_1,j_2} m\Gamma_k \left(\Omega_k + \frac{\Gamma_k}{4} \right), \tag{5.70}$$

and focus on $\omega_n \approx \Omega_k$ since the calculation depends on the Lindblad equation where the spectral density at Ω_k enters. In the limit where the coupling to external degrees of freedom is small $\Gamma_k \ll \Omega_k$ we find

$$\mathcal{G}^{j_1 j_2}_{M,BO}(\omega_n \approx \Omega_k) \approx \delta_{j_1,j_2} \frac{1}{2} J(\Omega_k). \tag{5.71}$$

Eq. (5.51) is the retarded bath Green's function that is in accordance with the Lindblad equation. With Eq. (5.38) and $\Omega_k \rightarrow i\omega$ we see that the result obtained from the reconstruction equation is in accordance with Eq. (5.51). Therefore, the reconstruction

equation is validated within this model system.

6. Conclusion

The advances in quantum hardware development raise the hope that in the near future artificial quantum systems can be used to solve problems that are computationally intractable for classical computers, even before a universal quantum computer exists. Analog quantum simulators, that mimic the quantum system of interest, and digital quantum simulators that simulate a time evolution using gates are promising ways for solving problems that are not solvable using classical computers.

An interesting case for quantum simulation is the simulation of molecules in context of the search for specialized chemicals. To pave the way to use the techniques presented in this thesis for the simulation of molecules on quantum simulators, we developed a software to describe molecules and simulate it on a quantum computer. This software was licensed by KIT.

A crucial requirement for quantum simulation is the reliability of the simulator. When trying to solve a problem using a quantum simulator that is not solvable in any other way, it is crucial to verify the validity based on the quantum simulator itself. The works presented in this thesis focus on the reliability of analog quantum simulators. They comprise simulators based on all possible physical realizations. Since the results should not be restricted to specific problems we made no assumptions concerning the Hamiltonian of the simulator. In addition, since they are very general system-bath considerations, the results of the works should be of interest beyond the field of quantum simulation.

Our approach to study the reliability of analog quantum simulations is based on the assumption that errors arise from coupling to external degrees of freedom. We described this using a system-bath approach, where the external degrees of freedom form the bath and the system describes the ideal simulator.

In chapter 3 we studied the reduced density matrix of the simulator in thermal equilibrium. A comparison to the ideal density matrix allowed us to make the influence of the external degrees of freedom tangible. We presented an equation of motion for the reduced density matrix and solved it in Laplace space. On one hand, we found a renormalization of energies, which can be calculated numerically or expressed approximately in terms of the self energy which incorporates the influence of external degrees of freedom. On the other hand, the eigenbasis changes due to the coupling to the bath, which can also be expressed in terms of the self energy. Exemplified on a one-qubit system, we showed that the change of the density matrix due to the environmental degrees of freedom has an influence on measurable quantities. Furthermore, we studied a six-qubit system, similar to the eight-qubit unit cell of a d-wave quantum annealer chip, to show that external degrees of freedom can have an influence on key quantum properties such as entanglement and coherence. In the context of analog quantum simulation, we learned from this work, which was presented in Ref. [VI], that the environment can substantially influence the density matrix of the simulator and, hence, the results of the simulation. After analyzing the influence of external degrees of freedom on the density matrix we focused on the calculation of measurable quantities. In chapter 4 we studied the influence of external degrees of freedom on an expectation value. In this work we allowed the system Hamiltonian to be time-dependent. With this, the work covers also digital quantum simulations. Based on a lowest-order perturbation expansion we presented a way to self-consistently study the reliability of an analog quantum simulator by additional measurements. This technique requires a rough knowledge of the decay properties of the bath. With this, it is possible to verify on which timescale the influence of the bath can be described in lowest order of the coupling to the external degrees of freedom. And it allows to estimate the size of the error. Therefore, it reveals the timescale in which a simulation is approximately reliable. Moreover, it can be used in the context of error mitigation methods that are based on lowest-order expansion as described in Ref. [25]. Reducing the error with this technique works only in a regime where the lowest-order correction scales linearly in time. With our self-consistent method it is possible to verify on which timescale this is true, so that the mitigation technique can be applied ben-

eficially. This work was presented in Ref. [V]. It is a contribution to the efforts to use artificial quantum systems to solve problems that are not solvable analytically or numerically using classical computers.

In chapter 5 we considered an analog quantum simulator in thermal equilibrium, where the result of the simulation is given by a correlator. Here, we focused on the correlator of the operator that mediates the coupling to the external degrees of freedom. In combination with the assumption that higher order correlators of this operator can be written in terms of two-time correlators, known as Wick's theorem, it allowed us to derive an equation that connects the perturbed correlator with the ideal one. With this equation it is possible to quantify the error induced by the external degrees of freedom and even to reconstruct the ideal result. Furthermore, we explain how to verify the assumption of Wick's theorem in an experiment. To perform the reconstruction it is necessary to characterize the correlator of the bath independently of the system. We discussed how imperfections in the correlator of the bath and in the perturbed correlator affect the result of the reconstruction. Especially, we showed that, although the reconstruction equation is valid in the limit of strong coupling, it is impossible to regain the ideal result in this limit, since even small errors in the measurement of the correlators have a huge impact. For the field of analog quantum simulation, this work, presented in Ref. [I], is a step towards simulations of systems, that are classically intractable. The central idea of this work that yields the reconstruction equation was transferred by L. Tian et al. [VII] to the question how measurement backaction influences the reliability of quantum simulation. The work of S. Zanker et al. [II] is based on a similar equation for fermionic systems which also allows for a reconstruction.

Both methods that allow for an estimation of errors, or even for a reconstruction, have the advantage that they bring no significant overhead to the quantum system, as it would be the case for quantum error correction. Hence, they can be realized in small quantum systems. Therefore, this thesis promotes the central effort of the quantum simulation community, namely, using near-term quantum systems to solve problems that cannot be solved using classical computers.

A. Disconnected diagrams

In Sec. 5.4 we express the perturbed Green's function using expectation values of the unperturbed system by introducing the time evolution operator in interaction picture $\mathcal{U}(\infty)$ (see also Sec. 2.4). To derive the Dyson equation that leads to the reconstruction equation we use the fact, that the so-called vacuum diagrams $\langle \mathcal{T}\mathcal{U}(\infty)\rangle_0$ cancel the disconnected diagrams in the correlator $\langle \mathcal{T}\mathcal{U}(\infty)\hat{O}(t)\hat{O}(0)\rangle_0$. The purpose of this appendix is to prove this. For simplicity, we carry out the derivation for the simple coupling Hamiltonian $H_C = \hat{O}\hat{X}$. A generalization to the full model (see Sec. (5.4)) is straight forward. In this appendix, we use the abbreviation $\hat{A}_i$ for $\hat{A}(t_i)$. Assuming $\langle \hat{O}(t)\rangle_0 = 0$ and $\langle \hat{X}(t)\rangle_0 = 0$ terms of odd order are zero and the vacuum diagrams are given by

$$\langle \mathcal{T}\mathcal{U}(\infty)\rangle_0 = \sum_n \frac{1}{n!}(-i)^n \int\limits_{-\infty}^{\infty} dt_1 \dots \int\limits_{-\infty}^{\infty} dt_n \, \langle \mathcal{T}\hat{O}_1 \dots \hat{O}_n\rangle_0 \, \langle \mathcal{T}\hat{X}_1 \dots \hat{X}_n\rangle_0 = \sum_n V_n \,, \tag{A.1}$$

Here, we have defined V_n as the vacuum diagrams of order n. Now we study the correlator $\langle \mathcal{T}\mathcal{U}(\infty)\hat{O}(t)\hat{O}(0)\rangle_0$ to express it in terms of the vacuum diagrams

$$\langle \mathcal{T}\mathcal{U}(\infty)\hat{O}_a\hat{O}_b\rangle_0 = \sum_n \frac{1}{n!}(-i)^n \int\limits_{-\infty}^{\infty} dt_1 \dots \int\limits_{-\infty}^{\infty} dt_n \, \langle \mathcal{T}\hat{O}_a\hat{O}_b\hat{O}_1 \dots \hat{O}_n\rangle_0 \, \langle \mathcal{T}\hat{X}_1 \dots \hat{X}_n\rangle_0 \,. \tag{A.2}$$

We apply Wick's theorem and select the two-time correlators that together form a connected diagram with external vertices. The surplus correlators are written as a higher

order correlator. From combinatorics it is known, that there are $\frac{n!}{(n-m)!}$ possibilities to choose m vertices out of n. This means, we find a connected diagram with m vertices $\frac{n!}{(n-m)!}$ times. This procedure leads to the following equation

$$\langle \mathcal{T}\mathcal{U}(\infty)\hat{O}_a\hat{O}_b\rangle_0 = \sum_n \frac{1}{n!}(-i)^n \int\limits_{-\infty}^{\infty} dt_1 \dots \int\limits_{-\infty}^{\infty} dt_n \sum_m^n \langle \mathcal{T}\hat{O}_a\hat{O}_1\rangle_0 \langle \mathcal{T}\hat{X}_1\hat{X}_2\rangle_0$$

$$\cdot \langle \mathcal{T}\hat{O}_2\hat{O}_3\rangle_0 \dots \langle \mathcal{T}\hat{X}_{m-1}\hat{X}_m\rangle_0 \langle \mathcal{T}\hat{O}_m\hat{O}_b\rangle_0$$

$$\cdot \frac{n!}{(n-m)!} \langle \mathcal{T}\hat{O}_{m+1}\dots\hat{O}_n\rangle_0 \langle \mathcal{T}\hat{X}_{m+1}\dots\hat{X}_n\rangle_0 . \quad \text{(A.3)}$$

In this expression, we can identify the vacuum diagrams of order $n-m$

$$\langle \mathcal{T}\mathcal{U}(\infty)\hat{O}_a\hat{O}_b\rangle_0 = \sum_n \sum_m^n$$

$$\cdot \underbrace{\underbrace{(-i)^m \int\limits_{-\infty}^{\infty} dt_1 \dots \int\limits_{-\infty}^{\infty} dt_m \langle \mathcal{T}\hat{O}_a\hat{O}_1\rangle_0 \langle \mathcal{T}\hat{X}_1\hat{X}_2\rangle_0 \langle \mathcal{T}\hat{O}_2\hat{O}_3\rangle_0 \dots \langle \mathcal{T}\hat{X}_{m-1}\hat{X}_m\rangle_0 \langle \mathcal{T}\hat{O}_m\hat{O}_b\rangle_0}_{=C_m^{a,b}}}_{=V_{n-m}}$$

$$\cdot \frac{1}{(n-m)!}(-i)^{n-m} \int\limits_{-\infty}^{\infty} dt_{m+1} \dots \int\limits_{-\infty}^{\infty} dt_n \langle \mathcal{T}\hat{O}_{m+1}\dots\hat{O}_n\rangle_0 \langle \mathcal{T}\hat{X}_{m+1}\dots\hat{X}_n\rangle_0 , \quad \text{(A.4)}$$

We express the conntected diagrams of order m going from time a to b as $C_m^{a,b}$, where $C_0^{a,b} = \langle \mathcal{T}\hat{O}_a\hat{O}_b\rangle_0$. It is possible to write the vacuum diagrams $\langle \mathcal{T}\mathcal{U}(\infty)\rangle_0$ as a prefactor using the Cauchy product formula

$$\langle \mathcal{T}\mathcal{U}(\infty)\hat{O}_a\hat{O}_b\rangle_0 = \sum_n^{\infty}\sum_m^n C_m^{a,b}V_{n-m} = \sum_m^{\infty} C_m^{a,b} \sum_n^{\infty} V_n = \langle \mathcal{T}\mathcal{U}(\infty)\rangle_0 \sum_m^{\infty} C_m^{a,b} . \quad \text{(A.5)}$$

With this we see, that the vacuum diagrams cancel the disconnected diagrams in the expression for the perturbed Green's function

$$\frac{\langle \mathcal{T}\mathcal{U}(\infty)\hat{O}_a\hat{O}_b\rangle_0}{\langle \mathcal{T}\mathcal{U}(\infty)\rangle_0} = \text{———} + \text{——\small{ooo}——} + \text{——\small{ooo}——\small{ooo}——} + \dots \ . \tag{A.6}$$

B. Four-time correlator and corrections to Wick's theorem

The assumption that Wick's theorem is valid for correlators of operator $\hat{O}$ is fundamental for the derivation of the reconstruction equation in chapter 5. In this section, we give the derivation for Eqs. (5.7) and (5.9), that allow us to validate the assumption of Wick's theorem in experiment. We introduce the lowest order correction to Wick's theorem $G_4(t_1, t_2, t_3, t_4)$,

$$G_4(t_1, t_2, t_3, t_4) = \langle \mathcal{T} \hat{O}_1 \hat{O}_2 \hat{O}_3 \hat{O}_4 \rangle_{0,F} - \langle \mathcal{T} \hat{O}_1 \hat{O}_2 \hat{O}_3 \hat{O}_4 \rangle_0 \tag{B.1}$$

$$= \langle \mathcal{T} \hat{O}_1 \hat{O}_2 \hat{O}_3 \hat{O}_4 \rangle_{0,F} - \sum_{\substack{3 \text{ perm.} \\ a,b,c,d}} \langle \mathcal{T} \hat{O}_a \hat{O}_b \rangle_0 \langle \mathcal{T} \hat{O}_c \hat{O}_d \rangle_0 \ , \tag{B.2}$$

This correction to Wick's theorem is described by the difference between the real four-time correlators where Wick's theorem is not valid and the four-time correlators where Wick's theorem is valid. For those correlators, Wick's theorem is applied and they are described as a sum of products of two-time correlators, where the sum runs over all three indistinguishable permutations. $\langle \ldots \rangle$ ($\langle \ldots \rangle_0$) describe (un)perturbed correlators where Wick's theorem is assumed to be valid. We introduce index F to indicate that $\langle \ldots \rangle_F$ ($\langle \ldots \rangle_{0,F}$) refer to the real correlators where Wick's theorem is not exactly valid. We study the deviations from Wick's theorem based on the simple coupling Hamiltonian $H_C = \hat{O}\hat{X}$. It is possible to directly generalize the results to the full model described in Sec. (5.4). To shorten the equations we introduce $\hat{A}_i$ as an abbreviation for $\hat{A}(t_i)$ and use the abbreviation $G_4(1, 2, 3, 4) = G_4(t_1, t_2, t_3, t_4)$. In the context of this work, we only consider terms in first order of G_4. Higher order contributions are neglected. With this,

an n-time correlator is given by

$$\langle \mathcal{T} \hat{O}_1 \dots \hat{O}_n \rangle_{0,F} = \langle \mathcal{T} \hat{O}_1 \dots \hat{O}_n \rangle_0 + \sum_{\substack{\text{perm.} \\ \alpha,\beta,\gamma,\delta}} G(\alpha,\beta,\gamma,\delta) \langle \mathcal{T} \prod_{k \in \{1,\dots n\} \setminus \{\alpha,\beta,\gamma,\delta\}} \hat{O}_k \rangle_0 . \quad \text{(B.3)}$$

In the next section, we show that Wick's theorem holds also for the perturbed correlators if it is true for the ideal correlators. From this, we look at perturbed four-time correlators and derive the lowest order correction to Wick's theorem for the full system. Finally, we derive an equation that connects the perturbed Green's function where Wick's theorem is not valid with the perturbed Green's function where we assume Wick's theorem to be valid. This equation shows, how to validate the assumption of Wick's theorem in experiment.

B.1. Wick's theorem for perturbed correlators

Assuming Wick's theorem holds for the free correlators, we show in this section, that it follows, that Wick's theorem is also true for the perturbed correlators. We write the perturbed four-time correlator using free correlators

$$\langle \mathcal{T} \hat{O}_\text{I} \hat{O}_\text{II} \hat{O}_\text{III} \hat{O}_\text{IV} \rangle = \frac{\langle \mathcal{T} \mathcal{U}(\infty) \hat{O}_\text{I} \hat{O}_\text{II} \hat{O}_\text{III} \hat{O}_\text{IV} \rangle_0}{\langle \mathcal{T} \mathcal{U}(\infty) \rangle_0} \quad \text{(B.4)}$$

$$= \sum_n \frac{(-i)^n}{n!} \int_{-\infty}^{\infty} \mathrm{d}t_1 \dots \int_{-\infty}^{\infty} \mathrm{d}t_n \frac{1}{\langle \mathcal{T} \mathcal{U}(\infty) \rangle_0} \langle \mathcal{T} \hat{O}_\text{I} \hat{O}_\text{II} \hat{O}_\text{III} \hat{O}_\text{IV} \hat{O}_1 \dots \hat{O}_n \rangle_0 \langle \mathcal{T} \hat{X}_1 \dots \hat{X}_n \rangle_0 .$$

$$\text{(B.5)}$$

In Appendix A we identified connected diagrams with m vertices $C_m^{a,b}$ and vacuum diagrams V_n of order n in similar terms. Here, we start with isolating connected diagrams $C_m^{a,b}$ with m vertices, which occure $\frac{n!}{(n-m)!}$ times. In this step, we have six indistinguishable ways to choose a and b out of $\text{I}, \text{II}, \text{III}, \text{IV}$. From the remaining $n-m$ operators we

identify connected diagrams with k vertices $C_k^{c,d}$, which occur $\frac{(n-m)!}{(n-m-k)!}$ times. Since for example $C_m^{\mathrm{I,II}}$ and $C_k^{\mathrm{I,II}}$ are indistinguishable for $m = k$, we are left with three indistinguishable permutations. The remaining operators form vacuum diagrams with $n-m-k$ vertices V_{n-m-k}. With this, we have

$$\langle \mathcal{T} \hat{O}_\mathrm{I} \hat{O}_\mathrm{II} \hat{O}_\mathrm{III} \hat{O}_\mathrm{IV} \rangle$$

$$= \sum_n \frac{(-i)^n}{n!} \int\limits_{-\infty}^{\infty} \mathrm{d}t_1 \dots \int\limits_{-\infty}^{\infty} \mathrm{d}t_n \frac{1}{\langle \mathcal{T}\mathcal{U}(\infty)\rangle_0} \sum_{\substack{3 \text{ perm.} \\ a,b}} \sum_m^n \frac{n!}{(n-m)!}$$

$$\cdot \langle \mathcal{T} \hat{O}_a \hat{O}_1 \rangle_0 \langle \mathcal{T} \hat{X}_1 \hat{X}_2 \rangle_0 \langle \mathcal{T} \hat{O}_2 \hat{O}_3 \rangle_0 \dots \langle \mathcal{T} \hat{O}_m \hat{O}_b \rangle_0$$

$$\cdot \sum_k^{n-m} \frac{(n-m)!}{(n-m-k)!} \langle \mathcal{T} \hat{O}_c \hat{O}_{m+1} \rangle_0 \langle \mathcal{T} \hat{X}_{m+1} \hat{X}_{m+2} \rangle_0 \langle \mathcal{T} \hat{O}_{m+2} \hat{O}_{m+3} \rangle_0 \dots \langle \mathcal{T} \hat{O}_{m+k} \hat{O}_d \rangle_0$$

$$\cdot \langle \mathcal{T} \hat{O}_{m+k+1} \dots \hat{O}_n \rangle_0 \langle \mathcal{T} \hat{X}_{m+k+1} \dots \hat{X}_n \rangle_0 \tag{B.6}$$

$$= \sum_{\substack{3 \text{ perm.} \\ a,b}} \frac{1}{\langle \mathcal{T}\mathcal{U}(\infty)\rangle_0} \sum_n^{\infty} \sum_m^n C_m^{a,b} \sum_k^{n-m} C_k^{c,d} \ V_{n-m-k} \tag{B.7}$$

$$= \sum_{\substack{3 \text{ perm.} \\ a,b}} \frac{1}{\langle \mathcal{T}\mathcal{U}(\infty)\rangle_0} \sum_n^{\infty} V_n \sum_m^{\infty} C_m^{a,b} \sum_k^{\infty} C_k^{c,d} \tag{B.8}$$

$$= \sum_{\substack{3 \text{ perm.} \\ a,b}} \langle \mathcal{T} \hat{O}_a \hat{O}_b \rangle \langle \mathcal{T} \hat{O}_c \hat{O}_d \rangle \ . \tag{B.9}$$

For the rearrangement of summations in Eq. (B.8) we make use of the Cauchy product formula for three series followed by an index shift. With this, we have shown, that the perturbed four-time correlator can be expressed as a sum of products of perturbed two-time correlators.

B.2. Correction to Wick's theorem for perturbed four-time correlators

In this section, we study the perturbed four-time correlator including corrections to Wick's theorem in lowest order in G_4. To analyze the correction to Wick's theorem for the full four-time correlator, we also have to take into account the correction to the normalization

$$\frac{1}{\langle \mathcal{T}\mathcal{U}(\infty)\rangle_{0,F}} = \frac{1}{\langle \mathcal{T}\mathcal{U}(\infty)\rangle_0 + \langle \mathcal{T}\mathcal{U}(\infty)\rangle_{0,\text{corr}}} \approx \frac{1}{\langle \mathcal{T}\mathcal{U}(\infty)\rangle_0} \left(1 - \frac{\langle \mathcal{T}\mathcal{U}(\infty)\rangle_{0,\text{corr}}}{\langle \mathcal{T}\mathcal{U}(\infty)\rangle_0} \right) .$$

(B.10)

We introduce the following abbreviation to record for which set of operators we apply Wick's theorem

$$\text{Wick}(A, \pi_n \backslash B, C) = \langle \mathcal{T} \prod_{k \in A \cup \pi_n \backslash B} \hat{O}_k \rangle_0 \, \langle \mathcal{T} \prod_{l \in \pi_n \cup C} \hat{X}_l \rangle_0 \, ,$$

(B.11)

where $\pi_n = \{1, \ldots, n\}$ represents the set of operators $\hat{O}_i$ and $\hat{X}_i$ for the given numbers. The first and third arguments are optional. If C is not given, it means that there are no additional bath operators to take into account. If the argument before the permutation symbol π_n is left out means that no additional operators $\hat{O}$ contribute.

Using this and Eq. (B.3) we can express the perturbed four-time correlator in lowest order in G_4

$$\langle \mathcal{T} \hat{O}_{\mathrm{I}} \hat{O}_{\mathrm{II}} \hat{O}_{\mathrm{III}} \hat{O}_{\mathrm{IV}} \rangle_F$$

$$= \sum_{\substack{3 \text{ perm.} \\ a,b,c,d}} \langle \mathcal{T} \hat{O}_a \hat{O}_b \rangle \langle \mathcal{T} \hat{O}_c \hat{O}_d \rangle - \sum_{\substack{3 \text{ perm.} \\ a,b,c,d}} \langle \mathcal{T} \hat{O}_a \hat{O}_b \rangle \langle \mathcal{T} \hat{O}_c \hat{O}_d \rangle \frac{\langle \mathcal{T} \mathcal{U}(\infty) \rangle_{0,\mathrm{corr}}}{\langle \mathcal{T} \mathcal{U}(\infty) \rangle_0} + G_4(\mathrm{I}, \mathrm{II}, \mathrm{III}, \mathrm{IV})$$

$$+ \sum_n \frac{(-i)^n}{n!} \int\limits_{-\infty}^{\infty} dt_1 \ldots \int\limits_{-\infty}^{\infty} dt_n \frac{1}{\langle \mathcal{T} \mathcal{U}(\infty) \rangle_0} \left(\sum_{\substack{4 \text{ perm.} \\ a-d}} \sum_{\substack{\text{perm.} \\ \delta}} G_4(a, b, c, \delta) \mathrm{Wick}(\{d\}, \pi_n \backslash \{\delta\}) \right.$$

$$+ \sum_{\substack{6 \text{ perm.} \\ a-d}} \sum_{\substack{\text{perm.} \\ \gamma,\delta}} G_4(a, b, \gamma, \delta) \mathrm{Wick}(\{c, d\}, \pi_n \backslash \{\gamma, \delta\})$$

$$+ \sum_{\substack{\text{perm.} \\ \alpha-\delta}} G_4(\alpha, \beta, \gamma, \delta) \mathrm{Wick}(\{a - d\}, \pi_n \backslash \{\alpha - \delta\})$$

$$+ \sum_{\substack{4 \text{ perm.} \\ a-d}} \sum_{\substack{\text{perm.} \\ \beta,\gamma,\delta}} G_4(a, \beta, \gamma, \delta) \mathrm{Wick}(\{b, c, d\}, \pi_n \backslash \{\beta, \gamma, \delta\}) \right). \tag{B.12}$$

The summations run over all indistinguishable permutations. The correction to the vacuum diagrams is given by

$$\frac{\langle \mathcal{T} \mathcal{U}(\infty) \rangle_{0,\mathrm{corr}}}{\langle \mathcal{T} \mathcal{U}(\infty) \rangle_0}$$

$$= \sum_n \frac{(-i)^n}{n!} \int\limits_{-\infty}^{\infty} dt_1 \ldots \int\limits_{-\infty}^{\infty} dt_n \frac{1}{\langle \mathcal{T} \mathcal{U}(\infty) \rangle_0} \sum_{\substack{\text{perm.} \\ \alpha-\delta}} G_4(\alpha, \beta, \gamma, \delta) \mathrm{Wick}(\pi_n \backslash \{\alpha - \delta\}). \tag{B.13}$$

We also express the perturbed two-time correlator in lowest order in G_4

$$\langle \mathcal{T} \hat{O}_a \hat{O}_b \rangle_F = \langle \mathcal{T} \hat{O}_a \hat{O}_b \rangle - \langle \mathcal{T} \hat{O}_a \hat{O}_b \rangle \frac{\langle \mathcal{T} \mathcal{U}(\infty) \rangle_{0,\text{corr}}}{\langle \mathcal{T} \mathcal{U}(\infty) \rangle_0}$$

$$+ \sum_n \frac{(-i)^n}{n!} \int_{-\infty}^{\infty} \mathrm{d}t_1 \ldots \int_{-\infty}^{\infty} \mathrm{d}t_n \frac{1}{\langle \mathcal{T} \mathcal{U}(\infty) \rangle_0} \left(\sum_{\substack{\text{perm.} \\ \gamma, \delta}} G_4(a, b, \gamma, \delta) \mathrm{Wick}(\pi_n \backslash \{\gamma, \delta\}) \right.$$

$$+ \sum_{\substack{2 \text{ perm.} \\ k,l}} \sum_{\substack{\text{perm.} \\ \beta,\gamma,\delta}} G_4(k, \beta, \gamma, \delta) \mathrm{Wick}(l, \pi_n \backslash \{\beta, \gamma, \delta\})$$

$$\left. + \sum_{\substack{\text{perm.} \\ \alpha-\delta}} G_4(\alpha, \beta, \gamma, \delta) \mathrm{Wick}(a, b, \pi_n \backslash \{\alpha - \delta\}) \right) . \tag{B.14}$$

To find the correction to Wick's theorem for the perturbed four-time correlator we calculate

$$\langle \mathcal{T} \hat{O}_{\mathrm{I}} \hat{O}_{\mathrm{II}} \hat{O}_{\mathrm{III}} \hat{O}_{\mathrm{IV}} \rangle_F - \sum_{\substack{3 \text{ perm.} \\ a,b}} \langle \mathcal{T} \hat{O}_a \hat{O}_b \rangle_F \langle \mathcal{T} \hat{O}_c \hat{O}_d \rangle_F . \tag{B.15}$$

Only terms with the same type of G_4 can cancel. Therefore, we have to compare those terms. We show the procedure at the example of $G_4(a, b, \gamma, \delta)$

$$\sum_n \frac{(-i)^n}{n!} \int_{-\infty}^{\infty} \mathrm{d}t_1 \ldots \int_{-\infty}^{\infty} \mathrm{d}t_n \frac{1}{\langle \mathcal{T} \mathcal{U}(\infty) \rangle_0} \left(\sum_{\substack{6 \text{ perm.} \\ a-d}} \sum_{\substack{\text{perm.} \\ \gamma,\delta}} G_4(a, b, \gamma, \delta) \mathrm{Wick}(\{c, d\}, \pi_n \backslash \{\gamma, \delta\}) \right.$$

$$\left. - \sum_{\substack{6 \text{ perm.} \\ a-d}} \sum_{\substack{\text{perm.} \\ \gamma,\delta}} G_4(a, b, \gamma, \delta) \mathrm{Wick}(\pi_n \backslash \{\gamma, \delta\}) \langle \mathcal{T} \hat{O}_c \hat{O}_d \rangle \right) . \tag{B.16}$$

The summation over six permutations in the last term is necessary, since $G_4(a, b, \gamma, \delta)$ appears in both two-time correlators that are multiplied. Due to the summation over

the perturbations of γ, δ we get a factor $\frac{n!}{(n-2)!}$. We introduce $\tilde{n} = n - 2$ because the first contribution occurs for $n = 2$. With this we find

$$\sum_{\substack{6 \text{ perm.} \\ a-d}} (-i)^2 \int\limits_{-\infty}^{\infty} \mathrm{d}t_{x_1} \int\limits_{-\infty}^{\infty} \mathrm{d}t_{x_2}\, G_4(a, b, x_1, x_2) \frac{1}{\langle \mathcal{T}\mathcal{U}(\infty)\rangle_0} \sum_{\tilde{n}} \frac{(-i)^{\tilde{n}}}{\tilde{n}!} \int\limits_{-\infty}^{\infty} \mathrm{d}t_1 \dots \int\limits_{-\infty}^{\infty} \mathrm{d}t_{\tilde{n}}$$

$$\cdot \left(\mathrm{Wick}(\{c,d\}, \pi_{\tilde{n}}, \{x_1, x_2\}) - \mathrm{Wick}(\pi_{\tilde{n}}, \{x_1, x_2\}) \langle \mathcal{T}\hat{O}_c\hat{O}_d\rangle \right) . \qquad \text{(B.17)}$$

In this terms diagrams of the following forms multiplied by appropriate vacuum diagrams appear

$$(\mathrm{I}): \quad \text{} \quad (\mathrm{II}): \quad \text{} \quad \text{} , \qquad \text{(B.18)}$$

The cross is the diagrammatic representation of G_4. In the first term, both kinds of diagrams appear. Tough, the second term has only contributions from diagrams of type (II). We define the following names to describe the leg- and ring-type diagrams

$$L_m^{x_1, a} = (-i)^m \int\limits_{-\infty}^{\infty} \mathrm{d}t_1 \dots \int\limits_{-\infty}^{\infty} \mathrm{d}t_m\, \langle \mathcal{T}\hat{X}_{x_1}\hat{X}_1\rangle_0 \langle \mathcal{T}\hat{O}_1\hat{O}_2\rangle_0 \langle \mathcal{T}\hat{X}_2\hat{X}_3\rangle_0 \dots \langle \mathcal{T}\hat{O}_m\hat{O}_a\rangle_0 \qquad \text{(B.19)}$$

$$\text{with} \quad L_0^{x_1, a} = 0 \qquad \text{(B.20)}$$

$$R_m^{x_1, x_2} = (-i)^m \int\limits_{-\infty}^{\infty} \mathrm{d}t_1 \dots \int\limits_{-\infty}^{\infty} \mathrm{d}t_m\, \langle \mathcal{T}\hat{X}_{x_1}\hat{X}_1\rangle_0 \langle \mathcal{T}\hat{O}_1\hat{O}_2\rangle_0 \langle \mathcal{T}\hat{X}_2\hat{X}_3\rangle_0 \dots \langle \mathcal{T}\hat{X}_m\hat{X}_{x_2}\rangle_0 . \qquad \text{(B.21)}$$

Identifying these structures in Eq. (B.17), finding the correct combinatorical factors, and using the Cauchy product formular shows us that the terms of type (II) are fully canceled. We are left with

$$\sum_{\substack{6 \text{ perm.} \\ a-d}} (-i)^2 \int\limits_{-\infty}^{\infty} \mathrm{d}t_{x_1} \int\limits_{-\infty}^{\infty} \mathrm{d}t_{x_2}\, G_4(a, b, x_1, x_2) \sum_l^{\infty} \sum_k^{\infty} L_l^{x_1, c} L_k^{x_2, d} . \qquad \text{(B.22)}$$

We proceed analogously with all kinds of G_4 terms and find

$$
\langle \mathcal{T} \hat{O}_{\mathrm{I}} \hat{O}_{\mathrm{II}} \hat{O}_{\mathrm{III}} \hat{O}_{\mathrm{IV}} \rangle_F
$$

$$
= \sum_{\substack{3 \text{ perm.} \\ a,b}} \langle \mathcal{T} \hat{O}_a \hat{O}_b \rangle_F \langle \mathcal{T} \hat{O}_c \hat{O}_d \rangle_F + G_4(\mathrm{I}, \mathrm{II}, \mathrm{III}, \mathrm{IV}) - i \sum_{\substack{4 \text{ perm.} \\ a-d}} \int_{-\infty}^{\infty} \mathrm{d}t_{x_1} \, G_4(a, b, c, x_1) \sum_k L_k^{x_1,d}
$$

$$
- \sum_{\substack{6 \text{ perm.} \\ a-d}} \int_{-\infty}^{\infty} \mathrm{d}t_{x_1} \int_{-\infty}^{\infty} \mathrm{d}t_{x_2} \, G_4(a, b, x_1, x_2) \sum_l \sum_k L_l^{x_1,c} L_k^{x_2,d}
$$

$$
+ i \sum_{\substack{4 \text{ perm.} \\ a-d}} \int_{-\infty}^{\infty} \mathrm{d}t_{x_1} \int_{-\infty}^{\infty} \mathrm{d}t_{x_2} \int_{-\infty}^{\infty} \mathrm{d}t_{x_3} \, G_4(a, x_1, x_2, x_3) \sum_l \sum_k \sum_m L_l^{x_1,b} L_k^{x_2,c} L_m^{x_3,d}
$$

$$
+ \int_{-\infty}^{\infty} \mathrm{d}t_{x_1} \int_{-\infty}^{\infty} \mathrm{d}t_{x_2} \int_{-\infty}^{\infty} \mathrm{d}t_{x_3} \int_{-\infty}^{\infty} \mathrm{d}t_{x_4} \, G_4(x_1, x_2, x_3, x_4) \sum_l \sum_k \sum_m \sum_n L_l^{x_1,a} L_k^{x_2,b} L_m^{x_3,c} L_m^{x_4,d} .
$$

$$
\tag{B.23}
$$

We introduce a diagrammatic representation for the remaining terms

$$
\mathsf{X} = \mathsf{X} + \mathsf{X}\!\!-\!\!-\!\!- + \mathsf{X}\!\!-\!\!-\!\!- + \mathsf{X}\!\!-\!\!-\!\!-\!\!- + \dots ,
\tag{B.24}
$$

and find the correction to Wick's theorem for the perturbed four-time correlator

$$
\langle \mathcal{T} \hat{O}_{\mathrm{I}} \hat{O}_{\mathrm{II}} \hat{O}_{\mathrm{III}} \hat{O}_{\mathrm{IV}} \rangle_F = \sum_{\substack{3 \text{ perm.} \\ a,b,c,d}} \langle \mathcal{T} \hat{O}_a \hat{O}_b \rangle_F \langle \mathcal{T} \hat{O}_c \hat{O}_d \rangle_F + \mathsf{X} .
\tag{B.25}
$$

B.3. Correction to Wick's theorem for Green's functions

In analogy to the calculation of the perturbed four-time correlator we find

$$
\langle \mathcal{T} \hat{O}_\mathrm{I} \hat{O}_\mathrm{II} \rangle_F = \langle \mathcal{T} \hat{O}_\mathrm{I} \hat{O}_\mathrm{II} \rangle - \int_{-\infty}^{\infty} \mathrm{d}t_{x_1} \int_{-\infty}^{\infty} \mathrm{d}t_{x_2} \, G_4(\mathrm{I}, \mathrm{II}, x_1, x_2) \sum_{k}^{\infty} R_k^{x_1, x_2}
$$

$$
+ \, i \sum_{\substack{2 \text{ perm:} \\ a,b}} \int_{-\infty}^{\infty} \mathrm{d}t_{x_1} \int_{-\infty}^{\infty} \mathrm{d}t_{x_2} \int_{-\infty}^{\infty} \mathrm{d}t_{x_3} \, G_4(a, x_1, x_2, x_3) \sum_{l}^{\infty} \sum_{k}^{\infty} R_k^{x_1, x_2} L_l^{x_3, b}
$$

$$
+ \int_{-\infty}^{\infty} \mathrm{d}t_{x_1} \int_{-\infty}^{\infty} \mathrm{d}t_{x_2} \int_{-\infty}^{\infty} \mathrm{d}t_{x_3} \int_{-\infty}^{\infty} \mathrm{d}t_{x_4} \, G_4(x_1, x_2, x_3, x_4) \sum_{l}^{\infty} \sum_{k}^{\infty} \sum_{m}^{\infty} R_k^{x_1, x_2} L_l^{x_3, \mathrm{I}} L_m^{x_4, \mathrm{II}}
$$

$$\tag{B.26}$$

$$
= \langle \mathcal{T} \hat{O}_\mathrm{I} \hat{O}_\mathrm{II} \rangle + \text{✕⟨} \,. \tag{B.27}
$$

List of tables

List of figures

Bibliography

1. Popkin, G. *Quest for qubits.* Science **354** (2016) (cit. on p. 9).

2. Taylor, J. M. *A quantum future awaits.* Science **361,** 313 (2018) (cit. on p. 9).

3. *Quantum possibilities.* Nat. Phys. **14,** 321 (2018) (cit. on p. 9).

4. Castelvecchi, D. *IBM's quantum cloud computer goes commercial.* Nature **543,** 159 (2017) (cit. on p. 9).

5. Georgescu, I. M., Ashhab, S. & Nori, F. *Quantum simulation.* Rev. Mod. Phys. **86,** 153 (2014) (cit. on pp. 9, 10).

6. DiVincenzo, D. P. *The physical implementation of quantum computation.* Fortschr. Phys. **48,** 771 (2000) (cit. on p. 9).

7. Barends, R., Kelly, J., Megrant, A., Veitia, A., Sank, D., Jeffrey, E., White, T. C., Mutus, J., Fowler, A. G., Campbell, B., Chen, Y., Chen, Z., Chiaro, B., Dunsworth, A., Neill, C., O'Malley, P., Roushan, P., Vainsencher, A., Wenner, J., Korotkov, A. N., Cleland, A. N. & Martinis, J. M. *Superconducting quantum circuits at the surface code threshold for fault tolerance.* Nature **508,** 500–503 (2014) (cit. on p. 9).

8. Preskill, J. *Quantum Computing in the NISQ era and beyond.* Quantum **2,** 79 (2018) (cit. on p. 9).

9. Lloyd, S. *Universal Quantum Simulators.* Science **273,** 1073–1078 (1996) (cit. on p. 10).

10. Britton, J. W., Sawyer, B. C., Keith, A. C., Wang, C.-C. J., Freericks, J. K., Uys, H., Biercuk, M. J. & Bollinger, J. J. *Engineered two-dimensional Ising interactions in a trapped-ion quantum simulator with hundreds of spins.* Nature **484,** 489–492 (2012) (cit. on p. 10).

11. Brumfiel, G. *Simulation: Quantum leaps.* Nature **491,** 322–324 (2012) (cit. on p. 10).

12. Struck, J., Ölschläger, C., Le Targat, R., Soltan-Panahi, P., Eckardt, A., Lewenstein, M., Windpassinger, P. & Sengstock, K. *Quantum Simulation of Frustrated Classical Magnetism in Triangular Optical Lattices.* Science **333,** 996–999 (2011) (cit. on p. 10).

13. Hart, R. A., Duarte, P. M., Yang, T.-L., Liu, X., Paiva, T., Khatami, E., Scalettar, R. T., Trivedi, N., Huse, D. A. & Hulet, R. G. *Observation of antiferromagnetic correlations in the Hubbard model with ultracold atoms.* Nature **519,** 211–214 (2015) (cit. on p. 10).

14. Alsing, P. M., Dowling, J. P. & Milburn, G. J. *Ion Trap Simulations of Quantum Fields in an Expanding Universe.* Phys. Rev. Lett. **94,** 220401 (2005) (cit. on p. 10).

15. García-Álvarez, L., Las Heras, U., Mezzacapo, A., Sanz, M., Solano, E. & Lamata, L. *Quantum chemistry and charge transport in biomolecules with superconducting circuits.* Scientific reports **6,** 27836 (2016) (cit. on pp. 10, 56, 59).

16. Hauke, P., Cucchietti, F. M., Tagliacozzo, L., Deutsch, I. & Lewenstein, M. *Can one trust quantum simulators?* Rep. Prog. Phys. **75,** 082401 (2012) (cit. on p. 10).

17. Cirac, J. I. & Zoller, P. *Goals and opportunities in quantum simulation.* Nat. Phys. **8,** 264–266 (2012) (cit. on pp. 10, 11).

18. Leibfried, D. *Could a boom in technologies trap Feynman's simulator?* Nature **463,** 608 (2010) (cit. on p. 10).

19. Trotzky, S., Pollet, L., Gerbier, F., Schnorrberger, U., Bloch, I., Prokof'ev, N. V., Svistunov, B. & Troyer, M. *Suppression of the critical temperature for superfluidity near the Mott transition.* Nat. Phys. **6,** 998–1004 (2010) (cit. on p. 11).

20. Jördens, R., Tarruell, L., Greif, D., Uehlinger, T., Strohmaier, N., Moritz, H., Esslinger, T., De Leo, L., Kollath, C., Georges, A., Scarola, V., Pollet, L., Burovski, E., Kozik, E. & Troyer, M. *Quantitative Determination of Temperature in the Approach to Magnetic Order of Ultracold Fermions in an Optical Lattice.* Phys. Rev. Lett. **104,** 180401 (2010) (cit. on p. 11).

21. Knee, G. C. & Munro, W. J. *Optimal Trotterization in universal quantum simulators under faulty control.* Phys. Rev. A **91,** 052327 (2015) (cit. on p. 11).

22. Sarovar, M., Zhang, J. & Zeng, L. *Reliability of analog quantum simulation.* EPJ quantum technology **4,** 1 (2017) (cit. on p. 11).

23. Hangleiter, D., Kliesch, M., Schwarz, M. & Eisert, J. *Direct certification of a class of quantum simulations.* Quantum Sci. Technol. **2,** 015004 (2017) (cit. on p. 11).

24. Li, Y. & Benjamin, S. C. *Efficient Variational Quantum Simulator Incorporating Active Error Minimization.* Phys. Rev. X **7,** 021050 (2017) (cit. on pp. 11, 46).

25. Temme, K., Bravyi, S. & Gambetta, J. M. *Error Mitigation for Short-Depth Quantum Circuits.* Phys. Rev. Lett. **119,** 180509 (2017) (cit. on pp. 11, 16, 46, 84).

26. Bonet-Monroig, X., Sagastizabal, R., Singh, M. & O'Brien, T. E. *Low-cost error mitigation by symmetry verification,* arXiv: 1807.10050 (2018) (cit. on p. 11).

27. Barends, R., Kelly, J., Megrant, A., Sank, D., Jeffrey, E., Chen, Y., Yin, Y., Chiaro, B., Mutus, J., Neill, C., O'Malley, P., Roushan, P., Wenner, J., White, T. C., Cleland, A. N. & Martinis, J. M. *Coherent Josephson Qubit Suitable for Scalable Quantum Integrated Circuits.* Phys. Rev. Lett. **111,** 080502 (2013) (cit. on p. 16).

28. Häffner, H., Roos, C. F. & Blatt, R. *Quantum computing with trapped ions.* Physics Reports **469,** 155–203 (2008) (cit. on p. 16).

29. Carmichael, H. J. *Statistical Methods in Quantum Optics 1: Master Equations and Fokker-Planck Equations* (Springer-Verlag Berlin Heidelberg, 1999) (cit. on pp. 16, 77, 78).

30. Deng, Q., Averin, D. V., Amin, M. H. & Smith, P. *Decoherence induced deformation of the ground state in adiabatic quantum computation.* Scientific reports **3,** 1479 (2013) (cit. on pp. 16, 18, 28, 29).

31. Schad, P., Narozhny, B. N., Schön, G. & Shnirman, A. *Nonequilibrium spin noise and noise of susceptibility.* Phys. Rev. B **90,** 205419 (2014) (cit. on p. 17).

32. Golubev, D. S., Marthaler, M., Utsumi, Y. & Schön, G. *Statistics of voltage fluctuations in resistively shunted Josephson junctions.* Phys. Rev. B **81,** 184516 (2010) (cit. on pp. 17, 65).

33. Lutchyn, R. M., Cywiński, Ł., Nave, C. P. & Das Sarma, S. *Quantum decoherence of a charge qubit in a spin-fermion model.* Phys. Rev. B **78,** 024508 (2008) (cit. on p. 17).

34. Catelani, G., Koch, J., Frunzio, L., Schoelkopf, R. J., Devoret, M. H. & Glazman, L. I. *Quasiparticle Relaxation of Superconducting Qubits in the Presence of Flux.* Phys. Rev. Lett. **106,** 077002 (2011) (cit. on pp. 17, 36).

35. Leppäkangas, J., Marthaler, M. & Schön, G. *Phase-dependent quasiparticle tunneling in Josephson junctions: Measuring the* $\cos\varphi$ *term with a superconducting charge qubit.* Phys. Rev. B **84,** 060505 (2011) (cit. on pp. 17, 36).

36. Jarzynski, C. *Nonequilibrium work theorem for a system strongly coupled to a thermal environment.* J. Stat. Mech. **2004,** P09005 (2004) (cit. on pp. 18, 28).

37. Zurek, W. H. *Pointer basis of quantum apparatus: Into what mixture does the wave packet collapse?* Phys. Rev. D **24,** 1516–1525 (1981) (cit. on pp. 20, 39).

38. Zurek, W. H. *Environment-induced superselection rules.* Phys. Rev. D **26,** 1862–1880 (1982) (cit. on pp. 20, 39).

39. Stenberg, M. P. V., Köhn, O. & Wilhelm, F. K. *Characterization of decohering quantum systems: Machine learning approach.* Phys. Rev. A **93,** 012122 (2016) (cit. on p. 21).

40. Rønnow, T. F., Wang, Z., Job, J., Boixo, S., Isakov, S. V., Wecker, D., Martinis, J. M., Lidar, D. A. & Troyer, M. *Defining and detecting quantum speedup.* Science **345,** 420–424 (2014) (cit. on p. 21).

41. Denchev, V. S., Boixo, S., Isakov, S. V., Ding, N., Babbush, R., Smelyanskiy, V., Martinis, J. & Neven, H. *What is the Computational Value of Finite-Range Tunneling?* Phys. Rev. X **6,** 031015 (2016) (cit. on p. 21).

42. Bylander, J., Gustavsson, S., Yan, F., Yoshihara, F., Harrabi, K., Fitch, G., Cory, D. G., Nakamura, Y., Tsai, J.-S. & Oliver, W. D. *Noise spectroscopy through dynamical decoupling with a superconducting flux qubit.* Nat. Phys. **7,** 565–570 (2011) (cit. on pp. 22, 46).

43. Harris, R., Johnson, M. W., Han, S., Berkley, A. J., Johansson, J., Bunyk, P., Ladizinsky, E., Govorkov, S., Thom, M. C., Uchaikin, S., Bumble, B., Fung, A., Kaul, A., Kleinsasser, A., Amin, M. H. S. & Averin, D. V. *Probing Noise in Flux Qubits via Macroscopic Resonant Tunneling.* Phys. Rev. Lett. **101,** 117003 (2008) (cit. on p. 22).

44. Lifschitz, E. M. & Pitajewski, L. P. *Statistische Physik Teil 2 Theorie des kondensierten Zustandes* (Akademie Verlag, 1992) (cit. on p. 22).

45. Rickayzen, G. *Green's Functions and Condensed Matter* (Academic Press, 1980) (cit. on pp. 22, 63).

46. <u>Conradi</u>, I. Deformation der Gleichgewichtsdichtematrix durch Kopplung an eine Umgebung (2014) (cit. on pp. 27, 29, 33, 36, 38).

47. Sarandy, M. S. & Lidar, D. A. *Adiabatic Quantum Computation in Open Systems.* Phys. Rev. Lett. **95,** 250503 (2005) (cit. on p. 28).

48. Ashhab, S., Johansson, J. R. & Nori, F. *Decoherence in a scalable adiabatic quantum computer.* Phys. Rev. A **74,** 052330 (2006) (cit. on p. 28).

49. Saito, K., Wubs, M., Kohler, S., Kayanuma, Y. & Hänggi, P. *Dissipative Landau-Zener transitions of a qubit: Bath-specific and universal behavior.* Phys. Rev. B **75,** 214308 (2007) (cit. on p. 28).

50. Dittrich, T., Hänggi, P., Ingold, G.-L., Kramer, B., Schön, G. & Zwerger, W. *Quantum transport and dissipation.* Chap. 3 and references within. (Wiley-Vch Weinheim, 1998) (cit. on p. 36).

51. Zanker, S. & Marthaler, M. *Qubit dephasing due to quasiparticle tunneling.* Phys. Rev. B **91,** 174504 (2015) (cit. on p. 36).

52. Schoeller, H. & Schön, G. *Mesoscopic quantum transport: Resonant tunneling in the presence of a strong Coulomb interaction.* Phys. Rev. B **50,** 18436 (1994) (cit. on pp. 36, 46).

53. Karlewski, C. & Marthaler, M. *Time-local master equation connecting the Born and Markov approximations.* Phys. Rev. B **90,** 104302 (2014) (cit. on p. 36).

54. Lanting, T., Przybysz, A. J., Smirnov, A. Y., Spedalieri, F. M., Amin, M. H., Berkley, A. J., Harris, R., Altomare, F., Boixo, S., Bunyk, P., Dickson, N., Enderud, C., Hilton, J. P., Hoskinson, E., Johnson, M. W., Ladizinsky, E., Ladizinsky, N., Neufeld, R., Oh, T., Perminov, I., Rich, C., Thom, M. C., Tolkacheva, E., Uchaikin, S., Wilson, A. B. & Rose, G. *Entanglement in a Quantum Annealing Processor.* Phys. Rev. X **4,** 021041 (2014) (cit. on p. 42).

55. Stewart, G. W. *On the adjugate matrix.* Linear Algebra Appl. **283,** 151–164 (1998) (cit. on p. 43).

56. Greenberger, D. M., Horne, M. A., Shimony, A. & Zeilinger, A. *Bell's theorem without inequalities.* American Journal of Physics **58,** 1131 (1998) (cit. on p. 43).

57. Stenberg, M. P. V. & Wilhelm, F. K. *Simultaneous model selection and parameter estimation: A superconducting qubit coupled to a bath of incoherent two-level systems.* Phys. Rev. A **94,** 052119 (2016) (cit. on p. 46).

58. Somma, R., Ortiz, G., Gubernatis, J. E., Knill, E. & Laflamme, R. *Simulating physical phenomena by quantum networks.* Phys. Rev. A **65,** 042323 (2002) (cit. on p. 50).

59. Wecker, D., Hastings, M. B., Wiebe, N., Clark, B. K., Nayak, C. & Troyer, M. *Solving strongly correlated electron models on a quantum computer.* Phys. Rev. A **92,** 062318 (2015) (cit. on p. 50).

60. Dallaire-Demers, P.-L. & Wilhelm, F. K. *Quantum gates and architecture for the quantum simulation of the Fermi-Hubbard model.* Phys. Rev. A **94,** 062304 (2016) (cit. on p. 50).

61. Weiss, U. *Quantum dissipative systems* (World scientific, 2012) (cit. on pp. 54, 55).

62. Mostame, S., Rebentrost, P., Eisfeld, A., Kerman, A. J., Tsomokos, D. I. & Aspuru-Guzik, A. *Quantum simulator of an open quantum system using superconducting qubits: exciton transport in photosynthetic complexes.* New J. Phys. **14,** 105013 (2012) (cit. on pp. 56, 58).

63. Du, L.-H., You, J. Q. & Tian, L. *Superconducting circuit probe for analog quantum simulators.* Phys. Rev. A **92,** 012330 (2015) (cit. on p. 62).

64. Streif, M., Buchleitner, A., Jaksch, D. & Mur-Petit, J. *Measuring correlations of cold-atom systems using multiple quantum probes.* Phys. Rev. A **94,** 053634 (2016) (cit. on p. 62).

65. Uhrich, P., Castrignano, S., Uys, H. & Kastner, M. *Noninvasive measurement of dynamic correlation functions.* Phys. Rev. A **96,** 022127 (2017) (cit. on p. 62).

66. `https://quantumexperience.ng.bluemix.net/qx/devices` (cit. on p. 62).

67. Bagrets, D. A. & Nazarov, Y. V. *Full counting statistics of charge transfer in Coulomb blockade systems.* Phys. Rev. B **67,** 085316 (2003) (cit. on p. 65).

68. Pekola, J. P. *Josephson Junction as a Detector of Poissonian Charge Injection.* Phys. Rev. Lett. **93,** 206601 (2004) (cit. on p. 65).

69. Flindt, C., Fricke, C., Hohls, F., Novotný, T., Netočný, K., Brandes, T. & Haug, R. J. *Universal oscillations in counting statistics.* Proc. Natl. Acad. Sci. USA **106,** 10116–10119 (2009) (cit. on p. 65).

70. Rice, J. *Mathematical statistics and data analysis* (Nelson Education, 2006) (cit. on p. 65).

71. Joubaud, S., Petrosyan, A., Ciliberto, S. & Garnier, N. B. *Experimental Evidence of Non-Gaussian Fluctuations near a Critical Point.* Phys. Rev. Lett. **100,** 180601 (2008) (cit. on p. 65).

72. Bramwell, S. T., Holdsworth, P. C. W. & Pinton, J.-F. *Universality of rare fluctuations in turbulence and critical phenomena.* Nature **396,** 552–554 (1998) (cit. on p. 65).

73. Pennetta, C., Alfinito, E., Reggiani, L. & Ruffo, S. Non-Gaussian resistance fluctuations in disordered materials. in *Noise in Complex Systems and Stochastic Dynamics.* **5471** (2004), 5471–10 (cit. on p. 65).

74. Beach, K. S. D., Gooding, R. J. & Marsiglio, F. *Reliable Padé analytical continuation method based on a high-accuracy symbolic computation algorithm.* Phys. Rev. B **61,** 5147 (2000) (cit. on p. 75).

75. Wolf, F. A., Go, A., McCulloch, I. P., Millis, A. J. & Schollwöck, U. *Imaginary-Time Matrix Product State Impurity Solver for Dynamical Mean-Field Theory.* Phys. Rev. X **5,** 041032 (2015) (cit. on p. 75).

76. Leib, M. & Hartmann, M. J. *Many body physics with coupled transmission line resonators.* Phys. Scr. **2013,** 014042 (2013) (cit. on p. 76).

77. Navarrete-Benlloch, C., de Vega, I., Porras, D. & Cirac, J. I. *Simulating quantum-optical phenomena with cold atoms in optical lattices.* New J. Phys. **13,** 023024 (2011) (cit. on p. 76).